Steel and Composite Structures, *Vol. 30, No. 6 (2019) 517-534*
DOI: https://doi.org/10.12989/scs.2019.30.6.517

Effect of out-of-plane defects on the postbuckling behavior of graphene sheets based on nonlocal elasticity theory

Ahmad Soleimani [*1,2], Kia Dastani [3], Amin Hadi [1] and Mohamad Hasan Naei [1]

[1] *School of Mechanical Engineering, College of Engineering, University of Tehran, Tehran, Iran*
[2] *Department of Mechanical Engineering, University of Jiroft, Jiroft, Iran*
[3] *Department of Mechanical Engineering, Sharif University of Technology, Tehran, Iran*

(*Received February 14, 2018, Revised December 16, 2018, Accepted March 8, 2019*)

Abstract. In this paper, the effects of inevitable out-of-plane defects on the postbuckling behavior of single-layered graphene sheets (SLGSs) under in-plane loadings are investigated based on nonlocal first order shear deformation theory (FSDT) and von-Karman nonlinear model. A generic imperfection function, which takes the form of the products of hyperbolic and trigonometric functions, is employed to model out-of-plane defects as initial geometrical imperfections of SLGSs. Nonlinear equilibrium equations are derived from the principle of virtual work and variational formulation. The postbuckling equilibrium paths of imperfect graphene sheets (GSs) are presented by solving the governing equations via isogeometric analysis (IGA) and Newton-Raphson iterative method. Finally, the sensitivity of the postbuckling behavior of GS to shape, amplitude, extension on the surface, and location of initial imperfection is studied. Results showed that the small scale and initial imperfection effects on the postbuckling behavior of defective SLGS are important and cannot be ignored.

Keywords: out-of-plane defect; graphene sheet; postbuckling; nonlocal elasticity; first order shear deformation theory; isogeometric analysis

1. Introduction

Recently, nanostructural elements such as graphene sheets (GSs) have attracted considerable attention from the researches community for their superior properties. GSs are new class of two-dimensional carbon nanostructures and duo to rapid developments in science and technology, especially in micro and nano-scale fields, are widely used in micro-electromechanical systems (MEMS) and nano-electromechanical systems (NEMS) for their excellent properties (Craighead 2000). Thus, determining the mechanical behaviors of graphene sheets is important and many researchers have focused on them in recent years (Ansari *et al*. 2012, Farajpour *et al*. 2013a, b, Jalali *et al*. 2016, Naderi and Saidi 2014).

In the past years, studies on graphene have been conducted in different areas such as fabrication methods of graphene sheets (Whitener and Sheehan 2014). It is well known that graphene sheets are experimentally fabricated and duo to restrictions in manufacturing and production processes, they are not generally perfect and some defects in different forms may exist in the GSs (Banhart *et al*. 2010). From experimental point of view (Hashimoto *et al*. 2004) and atomistic simulations (Ariza and Ortiz 2010), the existence of unavoidable defects in graphene structure is verified during the fabrication process. Different investigations have been shown that defects can change the perfect two-dimensional hexagonal lattice of graphene sheets. Moreover, physical, electrical and mechanical properties of graphene are sensitive to lattice imperfections (Ansari *et al*. 2012, Baimova *et al*. 2013, Fan *et al*. 2010, Jing *et al*. 2012, Kotakoski *et al*. 2014, Lehmann *et al*. 2013, Lherbier *et al*. 2011, Neek-Amal and Peeters 2012, Wang *et al*. 2013, Xiao *et al*. 2009, 2010).

The defects of graphene structure are classified as (i) incomplete bonding defects by removing carbon atoms (vacancies), (ii) heterogeneous defects by adding carbon atoms or other impurities (adatoms), and (iii) topological defects by rearrangement of existing carbon atoms (different ring sizes like Stone-Wales (SW) defects made by rotating of a carbon bond). The effects of various types of defects on elastic properties of graphene sheets were investigated by different researchers (Ansari *et al*. 2011, 2012, Hao *et al*. 2008, Ito and Okamoto 2012, Neek-Amal and Peeters 2010b, Wang *et al*. 2013). Most of researchers reported the influence of SW defects on physical and mechanical properties of graphene using atomistic and continuum computational methods (Baimova *et al*. 2013, Fan *et al*. 2010, Lusk *et al*. 2010, Ma *et al*. 2009, Partovi-Azar *et al*. 2013, Rodrigues *et al*. 2011, Sun *et al*. 2012, Wang *et al*. 2013, Xiao *et al*. 2009, 2010).

The understanding of GSs stability response is important due to this fact that some potential applications of graphene sheets such as NEMS, flexible electronics and composite materials are related to its compressive or buckling responses. Many studies have been conducted on the buckling and postbuckling behaviors of the perfect

*Corresponding author, Ph.D., Professor,
E-mail: a.soleimani@ujiroft.ac.ir;
amd_soleimani@ut.ac.ir

ISSN: 1229-9367 (Print), 1598-6233 (Online)

graphene sheets (Ansari and Sahmani 2013, Ansari *et al*. 2013, Chandra *et al*. 2011, Farajpour *et al*. 2012, 2013a, b, Karličić *et al*. 2014, Mahdavi *et al*. 2012, Mohammadi *et al*. 2014, Naderi and Saidi 2014, Pradhan 2009, Rouhi and Ansari 2012). Despite the existence of numerous investigations on the physical and mechanical properties of defective graphene, to the authors' knowledge, the buckling behavior of defective graphene have been studied in few works (Montazeri *et al*. 2015, Neek-Amal and Peeters 2010a, 2012). The effect of grain boundary on the buckling response of graphene nanoribbons (GNRs) was investigated by Neek-Amal *et al*. (Neek-Amal and Peeters 2012) via MD simulations. Ebrahimi (2015) studied the effect of SW defects orientations and SW concentration on the buckling of GNRs using MD simulations.

Since the experimental studies of nanostructures are difficult, the simulations have become the prominent tool in order to model and study the nanostructures and their mechanical behaviors. Generally, the simulations can be classified into three main categories: (i) bottom-up simulations; (ii) the hybrid of bottom-up simulations; and (iii) top-down simulations. Atomistic lattice dynamics, molecular dynamics simulations (Brodka *et al*. 2007, Tang *et al*. 2008), and hybrid simulations (Bodily and Sun 2003, Li and Chou 2003a, b) belong to first two categories and are computationally expensive. Therefore, their application to the structures with small atoms and molecules are limited and are not suitable for analyzing large scale systems. The continuum simulations (Dastjerdi and Jabbarzadeh 2016, Radić and Jeremić 2016) which belong to the top-down simulations category, are less computationally expensive relative to the former two simulations categories. Thus, the continuum modeling simulations have been widely used for the study of nanostructures (Apuzzo *et al*. 2017, Bağdatlı 2015, Dastjerdi *et al*. 2016).

The original or classical continuum modeling cannot capture the small size effect in small-scale nanostructures and its application may lead to erroneous results, since the continuum assumption may not valid in the small scales (Adeli *et al*. 2017, Ansari *et al*. 2015, Daneshmehr *et al*. 2015, Farajpour *et al*. 2018, Hadi *et al*. 2018a, b, c, Hosseini *et al*. 2018, Nejad and Hadi 2016a, b, Nejad *et al*. 2017, Norouzzadeh and Ansari 2018a, Zargaripoor *et al*. 2018a, b). A number of continuum-based theories such as nonlocal elasticity (Bağdatlı 2015, Eringen 1983, 2002), strain gradient elasticity (Fleck and Hutchinson 1997, Jamalpoor and Hosseini 2015) and couple stress (Jung *et al*. 2014, Toupin 1962) have been proposed to account the size effect in the micro or nano-scale structures. Nonlocal elasticity theory introduced by Eringen (2002), have been widely applied to analyze many nanostructures problems and unlike classical continuum models, it assumes that the stress at a reference point is a function of strain field at all of points in the body. Both atomistic simulation results and experimental observations on phonon dispersion have shown the accuracy of this observation. According to this theory, a stress–strain relationship for a homogeneous elastic solid is

$$\sigma_{ij}^{nl} = \int_{v} \alpha\left(|x' - x|, \mu\right)\sigma_{ij}^{l} dv\left(x'\right)$$

where α is the nonlocal modulus or kernel function. It contains the small-scale effects incorporating into constitutive equations the nonlocal effects at the reference point x produced by local strain at the source x' and μ is a material constant that depends on internal and external characteristic length such as the lattice spacing and wavelength. Also, σ^{nl} is the nonlocal stress tensor at the reference point and σ^{l} is the classical stress tensor at local point. By appropriate choice of the kernel function, Eringen showed that the nonlocal constitutive equation given in integral form can be represented, for unbounded domains, in an equivalent differential form as

$$\left(1 - \mu\nabla^2\right)\sigma^{nl} = C : \varepsilon$$

Differential model of nonlocal elasticity theory has been widely used to study nanostructures behavior. Some previous studies indicated that in some cases differential form of nonlocal theory results in inconsistent prediction of nanostructure behavior. So, some researchers suggested integral form of nonlocal theory for such cases (Ansari *et al*. 2018). Recently Integral form of nonlocal elasticity is employed to investigate bending of nano-scale Timoshenko beams (Norouzzadeh and Ansari 2017) and nanoplates (Ansari *et al*. 2018). Also Norouzzadeh *et al*. (2017) have studied pre-buckling responses of Timoshenko nanobeams using both differential and integral form of Eringen's nonlocal elasticity theory and compared the results.

It has been shown that the nonlocal elasticity theory is quite accurate and reliable for the free vibration and buckling analysis of SLGSs and nanostructures by employing molecular dynamics modeling (Ahouel *et al*. 2016, Ansari and Sahmani 2013, Ansari *et al*. 2010, Arda and Aydogdu 2018, Belkorissat *et al*. 2015, Bounouara *et al*. 2016, Daneshmehr *et al*. 2015, Jandaghian and Rahmani 2017, Li and Hu 2015, 2016, Li *et al*. 2016a, b; Nejad and Hadi 2016a, b, Nejad *et al*. 2016, Rahmani *et al*. 2017, Uzun *et al*. 2018). In another work, Farajpour *et al*. (2013a reported that the results of nonlocal plate theory with consideration of surface effects are in good agreement with those of MD simulations for the buckling of circular single-layered graphene sheets. Many buckling studies based on nonlocal elasticity are reported in the literatures (Ansari and Sahmani 2013, Ansari *et al*. 2013, Farajpour *et al*. 2012, 2013b, Mohammadi *et al*. 2014, Pradhan 2009) for the study of perfect graphene nanoplates subjected to the mechanical loading. In the past few years, some investigations have been performed on the postbuckling behavior of graphene sheets based on the nonlocal elasticity (Farajpour *et al*. 2013a, Naderi and Saidi 2014). In all of the past investigations, the graphene sheet was considered as a perfect nanoplate.

According to the literature, graphene sheets may be defected and as far as the authors aware, there is no published work for postbuckling behavior of defective graphene sheet. Therefore, this paper investigates the effect of out-of-plane defects on the postbuckling behavior of single-layered graphene sheets (SLGSs) based on nonlocal first order shear deformation theory (FSDT) and von-Karman model. In this work, the nonlocal elasticity theory

is applied to study the small scale effects. The out-of-plane defect as an initial imperfection is considered by employing a generic imperfection function (Jalali *et al*. 2016) and nonlinear equilibrium equations are derived from the principle of virtual work.

The isogeometric analysis (IGA) based on non-uniform rational B-splines (NURBS) basis functions introduced by Hughes *et al*. (2005) which fulfills a gap between (CAD) and finite element analysis (FEA) and Newton-Raphson iterative method are used to determine the postbuckling equilibrium path of imperfect graphene sheets. IGA is a very robust and efficient numerical approach and have been used for analyzing of plates (Ansari and Norouzzadeh 2016, Fantuzzi and Tornabene 2016, Farzam-Rad *et al*. 2017, Le-Manh and Lee 2014, Nguyen-Xuan *et al*. 2013, 2014, Norouzzadeh and Ansari 2018b, Soleimani *et al*. 2016, Tran *et al*. 2013, Yin *et al*. 2016) recently. Standard finite element analysis uses Lagrange polynomials for approximation of both geometry and unknown solution field while IGA employs basis functions such as NURBS which are common in CAD approaches to describe the geometry for approximation of the physical response in an isoparametric sense. In other words, the IGA method uses the same basis functions for the approximation of both the geometry and unknown field variables, e.g., deflection in our case. The IGA method have many advantage features including, exact modeling of complex geometries with curved boundary, smoothness and higher order continuity, avoiding shear locking in very thin plates, simple meshing and mesh refinement (Ansari and Norouzzadeh 2016). Moreover, in contrast to regular finite element methods, the total degrees-of-freedom are reduced in IGA method which results in reducing of computational efforts. In this study, the IGA method was employed for nonlocal postbuckling analysis of imperfect graphene sheet due to its good inherent characteristics. Finally, the influence of shape, amplitude, extension on the surface, and location of initial imperfection and nonlocal parameter on the postbuckling behavior of SLGSs are studied. The results would be useful for the engineering design of graphene-based nano-structures.

2. Analysis

2.1 Numerical simulation procedure

Consider a rectangular single layered graphene sheet under compressive in-plane loading in the x and y directions (Fig. 1). The graphene sheet is modelled as orthotropic continuum plate with length a, width b, effective thickness h, and initial geometrical imperfection $w^*(x, y)$. The Cartesian coordinates system (x, y, z) is located at the corner of plate in the reference state.

It is supposed that the defective nanoplate is in a stress-free state and only transverse direction is considered for the initial geometric imperfection. In order to consider the effect of shear deformation through-the-thickness of plate and improving the accuracy of the results, according to the

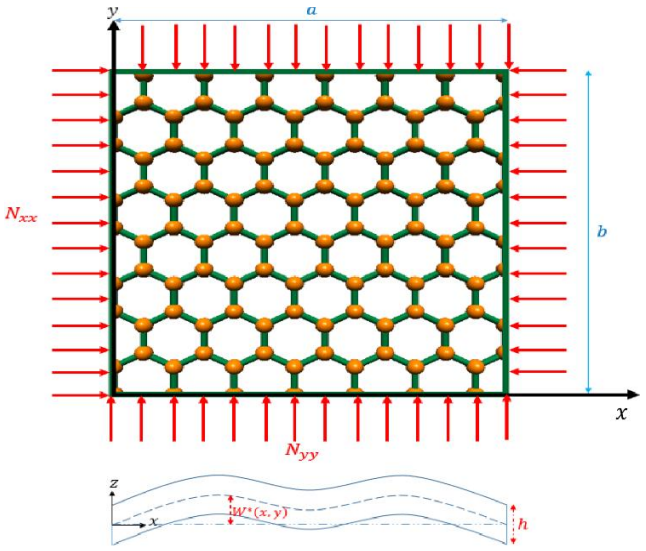

Fig. 1 Schematic diagram of imperfect GS subjected to in-plane loading.

first order shear deformation theory, the displacements field can be written as follows

$$\begin{cases} u = u_0(x,y) + z\phi_x \\ v = v_0(x,y) + z\phi_y \\ w = w_0(x,y) + w^*(x,y) \end{cases} \tag{1}$$

where u_0, v_0, w_0, ϕ_x and ϕ_y are the mid-plane displacement components of plate in the x, y, and z directions and rotations around y and x axes, respectively. $w^*(x, y)$ is the initial displacement of the mid-plane in transverse direction. The strain-displacement relations in the von-Karman form are defined as

$$\begin{Bmatrix} \varepsilon_{xx} \\ \varepsilon_{yy} \\ \gamma_{yz} \\ \gamma_{xz} \\ \gamma_{xy} \end{Bmatrix} = \begin{Bmatrix} \varepsilon^0_{xx} \\ \varepsilon^0_{yy} \\ \gamma^0_{yz} \\ \gamma^0_{xz} \\ \gamma^0_{xy} \end{Bmatrix} + z \begin{Bmatrix} \varepsilon^1_{xx} \\ \varepsilon^1_{yy} \\ \gamma^1_{yz} \\ \gamma^1_{xz} \\ \gamma^1_{xy} \end{Bmatrix} \tag{2}$$

where

$$\begin{Bmatrix} \varepsilon^0_{xx} \\ \varepsilon^0_{yy} \\ \gamma^0_{yz} \\ \gamma^0_{xz} \\ \gamma^0_{xy} \end{Bmatrix} = \begin{Bmatrix} \dfrac{\partial u_0}{\partial x} + \dfrac{1}{2}\left(\dfrac{\partial w_0}{\partial x}\right)^2 + \dfrac{\partial w_0}{\partial x}\dfrac{\partial w^*}{\partial x} \\ \dfrac{\partial v_0}{\partial y} + \dfrac{1}{2}\left(\dfrac{\partial w_0}{\partial y}\right)^2 + \dfrac{\partial w_0}{\partial y}\dfrac{\partial w^*}{\partial y} \\ \dfrac{\partial (w_0 + w^*)}{\partial y} + \phi_y \\ \dfrac{\partial (w_0 + w^*)}{\partial x} + \phi_x \\ \dfrac{\partial u_0}{\partial y} + \dfrac{\partial v_0}{\partial x} + \dfrac{\partial w_0}{\partial x}\dfrac{\partial w_0}{\partial y} + \dfrac{\partial w_0}{\partial x}\dfrac{\partial w^*}{\partial y} + \dfrac{\partial w^*}{\partial x}\dfrac{\partial w_0}{\partial y} \end{Bmatrix}, \tag{3}$$

$$\begin{Bmatrix} \varepsilon_{xx}^1 \\ \varepsilon_{yy}^1 \\ \gamma_{yz}^1 \\ \gamma_{xz}^1 \\ \gamma_{xy}^1 \end{Bmatrix} = \begin{Bmatrix} \dfrac{\partial \phi_x}{\partial x} \\ \dfrac{\partial \phi_y}{\partial y} \\ 0 \\ 0 \\ \dfrac{\partial \phi_x}{\partial y} + \dfrac{\partial \phi_y}{\partial x} \end{Bmatrix} \tag{3}$$

According to Eringen (1983), the nonlocal constitutive equation is written in the following differential form

$$\left(1-\mu\nabla^2\right)\sigma^{nl} = \sigma^{l}, \quad \sigma^{l} = C:\varepsilon, \quad \nabla^2 = \frac{\partial^2}{\partial x^2} + \frac{\partial^2}{\partial y^2} \tag{4}$$

where σ^{nl} and σ^{l} are the nonlocal stress tensor at the reference point and the classical stress tensor at the local point, respectively. Also $\mu = (e_0 a_0)^2$ is nonlocal parameter where e_0 is a material constant and a_0 is the internal characteristic length. C is the fourth-order elasticity tensor and ':' denotes the double dot product. Using Eq. (4), the stress-strain relations can be expressed for a nonlocal orthotropic graphene sheet as Eq. (5). In which components Q_{ij} (i, j = 1, 2, 4, 5, 6) are the elastic properties of the graphene sheet and can be defined as Eq. (6), where E, G and υ are Young's modulus, shear modulus and Poisson's ratio of plate, respectively.

The stress resultants N_{ij}^{nl}, M_{ij}^{nl} and Q_k^{nl} are expressed by Eqs. (7)-(9). In Eq. (8) k_s the transverse shear correction coefficient. By substituting Eq. (5) into Eqs. (7)-(9), the nonlocal constitutive relations are derived as Eqs. (10)-(12). The coefficients A_{ij} and D_{ij} in Eqs. (10)-(12) are expressed as Eqs. (13)-(15).

$$\begin{Bmatrix} \sigma_{xx}^{nl} \\ \sigma_{yy}^{nl} \\ \sigma_{yz}^{nl} \\ \sigma_{xz}^{nl} \\ \sigma_{xy}^{nl} \end{Bmatrix} - \mu\nabla^2 \begin{Bmatrix} \sigma_{xx}^{nl} \\ \sigma_{yy}^{nl} \\ \sigma_{yz}^{nl} \\ \sigma_{xz}^{nl} \\ \sigma_{xy}^{nl} \end{Bmatrix} = \begin{bmatrix} Q_{11} & Q_{12} & 0 & 0 & 0 \\ Q_{21} & Q_{22} & 0 & 0 & 0 \\ 0 & 0 & Q_{44} & 0 & 0 \\ 0 & 0 & 0 & Q_{55} & 0 \\ 0 & 0 & 0 & 0 & Q_{66} \end{bmatrix} \begin{Bmatrix} \varepsilon_{xx} \\ \varepsilon_{yy} \\ \gamma_{yz} \\ \gamma_{xz} \\ \gamma_{xy} \end{Bmatrix} \tag{5}$$

$$Q_{11} = \frac{E_1}{1-\nu_{12}\nu_{21}}, \quad Q_{22} = \frac{E_2}{1-\nu_{12}\nu_{21}}, \quad Q_{12} = \frac{\nu_{12}E_2}{1-\nu_{12}\nu_{21}}$$
$$Q_{21} = Q_{12}, \quad Q_{44} = G_{23}, \quad Q_{55} = G_{31}, \quad Q_{66} = G_{12} \tag{6}$$

$$(N_{xx}, N_{yy}, N_{xy})^{nl} = \int_{-\frac{h}{2}}^{\frac{h}{2}} (\sigma_{xx}, \sigma_{yy}, \sigma_{xy})^{nl}\, dz \tag{7}$$

$$(Q_x, Q_y)^{nl} = k_s \int_{-\frac{h}{2}}^{\frac{h}{2}} (\sigma_{xz}, \sigma_{yz})^{nl}\, dz \tag{8}$$

$$(M_{xx}, M_{yy}, M_{xy})^{nl} = \int_{-\frac{h}{2}}^{\frac{h}{2}} z\,(\sigma_{xx}, \sigma_{yy}, \sigma_{xy})^{nl}\, dz \tag{9}$$

$$\begin{Bmatrix} N_{xx}^{nl} \\ N_{yy}^{nl} \\ N_{xy}^{nl} \end{Bmatrix} - \mu\nabla^2 \begin{Bmatrix} N_{xx}^{nl} \\ N_{yy}^{nl} \\ N_{xy}^{nl} \end{Bmatrix} = \begin{bmatrix} A_{11} & A_{12} & 0 \\ A_{21} & A_{22} & 0 \\ 0 & 0 & A_{66} \end{bmatrix} \begin{Bmatrix} \varepsilon_{xx}^0 \\ \varepsilon_{yy}^0 \\ \gamma_{xy}^0 \end{Bmatrix} \tag{10}$$

$$\begin{Bmatrix} Q_y^{nl} \\ Q_x^{nl} \end{Bmatrix} - \mu\nabla^2 \begin{Bmatrix} Q_x^{nl} \\ Q_y^{nl} \end{Bmatrix} = \begin{bmatrix} A_{44} & 0 \\ 0 & A_{55} \end{bmatrix} \begin{Bmatrix} \gamma_{yz}^0 \\ \gamma_{xz}^0 \end{Bmatrix} \tag{11}$$

$$\begin{Bmatrix} M_{xx}^{nl} \\ M_{yy}^{nl} \\ M_{xy}^{nl} \end{Bmatrix} - \mu\nabla^2 \begin{Bmatrix} M_{xx}^{nl} \\ M_{yy}^{nl} \\ M_{xy}^{nl} \end{Bmatrix} = \begin{bmatrix} D_{11} & D_{12} & 0 \\ D_{21} & D_{22} & 0 \\ 0 & 0 & D_{66} \end{bmatrix} \begin{Bmatrix} \varepsilon_{xx}^1 \\ \varepsilon_{yy}^1 \\ \gamma_{xy}^1 \end{Bmatrix} \tag{12}$$

$$\begin{bmatrix} A_{11} & A_{12} & 0 \\ A_{21} & A_{22} & 0 \\ 0 & 0 & A_{66} \end{bmatrix} = h \begin{bmatrix} Q_{11} & Q_{12} & 0 \\ Q_{21} & Q_{22} & 0 \\ 0 & 0 & Q_{66} \end{bmatrix} \tag{13}$$

$$\begin{bmatrix} A_{44} & 0 \\ 0 & A_{55} \end{bmatrix} = h \begin{bmatrix} Q_{44} & 0 \\ 0 & Q_{55} \end{bmatrix} \tag{14}$$

$$\begin{bmatrix} D_{11} & D_{12} & 0 \\ D_{21} & D_{22} & 0 \\ 0 & 0 & D_{66} \end{bmatrix} = \frac{h^3}{12} \begin{bmatrix} Q_{11} & Q_{12} & 0 \\ Q_{21} & Q_{22} & 0 \\ 0 & 0 & Q_{66} \end{bmatrix} \tag{15}$$

Principle of virtual work is independent of constitutive relations. So by using the principle of virtual work and considering the small scale effect, the nonlocal governing equations based on first order shear deformation plate theory can be obtained as Eqs. (16)-(20).

$$\frac{\partial N_{xx}^{nl}}{\partial x} + \frac{\partial N_{xy}^{nl}}{\partial y} = 0 \tag{16}$$

$$\frac{\partial N_{xy}^{nl}}{\partial x} + \frac{\partial N_{yy}^{nl}}{\partial y} = 0 \tag{17}$$

$$\frac{\partial}{\partial x}\left[N_{xx}\frac{\partial(w_0+w^*)}{\partial x} + N_{xy}\frac{\partial(w_0+w^*)}{\partial y}\right] + \frac{\partial}{\partial y}\left[N_{xy}\frac{\partial(w_0+w^*)}{\partial x} + N_{yy}\frac{\partial(w_0+w^*)}{\partial y}\right] + \frac{\partial Q_x^{nl}}{\partial x} + \frac{\partial Q_y^{nl}}{\partial y} = 0 \tag{18}$$

$$\frac{\partial M_{xx}^{nl}}{\partial x} + \frac{\partial M_{xy}^{nl}}{\partial y} - Q_x^{nl} = 0 \tag{19}$$

$$\frac{\partial M_{xy}^{nl}}{\partial x} + \frac{\partial M_{yy}^{nl}}{\partial y} - Q_y^{nl} = 0 \tag{20}$$

2.2 Variational form

First, both sides of the above governing equations Eqs. (16)-(20) are multiplied by the first term of Eq. (4), $(1-\mu\Delta^2)$. Then, the weak form of the governing equations is obtained by pre-multiplying the equations of motion with δu_0, δv_0, δw_0, $\delta\phi_x$ and $\delta\phi_y$ respectively and integrating by parts over the element domain. Substituting force, moment and shear force resultants in the governing equations would result in variational form of equation which are presented in Appendix A.

2.3 Isogeometric analysis

In this section, the concept of NURBS-based IGA which firstly presented by Hughes *et al*. (2005) and Cottrell *et al*. (2009), will be briefly reviewed. More details of B-spline functions can be found in reference (Piegl and Tiller 2012). NURBS are generalization of B-spline functions with a prescribed degree of continuity which can be applied for constructing the shape functions. A NURBS curve is defined as

$$\mathbf{C}(\xi)=\frac{\sum_{i=1}^{n}N_{i,p}(\xi)w_i\mathbf{B}_i}{\sum_{i=1}^{n}N_{i,p}(\xi)w_i}=\sum_{i=1}^{n}R_i^p(\xi)\mathbf{B}_i \tag{21}$$

where $\mathbf{B}_i$, w_i and n are the i-th control point, individual weight for $\mathbf{B}_i$, and total number of control points, respectively. $N_{i,p}(\xi)$ is the i-th one-dimensional B-spline basis function of order p with knot value ξ which is defined as a series of non-decreasing real numbers in the parametric space of the knot vector, Ξ

$$\Xi=\left\{\xi_1,\xi_2,...,\xi_{n+p+1}\right\} \tag{22}$$

where ξ_i is the i-th knot, i (i = 1, 2,..., $n+p+1$) is the knot index, p is the order of the B-spline, and n is the number of basis functions. The interval $[\xi_1, \xi_{n+p+1}]$ and the half-open interval $[\xi_i, \xi_{i+1}]$ are called patch and the i-th knot span, respectively. A knot vector is referred as uniform if its knots are equally spaced. It can be noted that if more than one knot may be placed at the same location in the parametric space, the basis functions are C^{p-m} continuous at that location, where m is the multiplicity of the knot. In the isogeometric analysis, in order to satisfy the kronecker delta property at the boundary points, an open knot vector (a knot vector with p+1 repeated knots at the ends) is used. B-spline basis functions of order p are constructed using the Cox-de Boor recursion formula (Piegl and Tiller 2012)

$$N_{i,0}(\xi)=\begin{cases}1 & if\ \ \xi_i\le\xi\le\xi_{i+1}\\ 0 & otherwise\end{cases} \tag{23}$$

and for $p\ge 1$

$$N_{i,\mathrm{p}}(\xi)=\frac{\xi-\xi_i}{\xi_{i+p}-\xi_i}N_{i,\mathrm{p}-1}(\xi)+\frac{\xi_{i+p+1}-\xi}{\xi_{i+p+1}-\xi_{i+1}}N_{i+1,\mathrm{p}-1}(\xi) \tag{24}$$

B-spline functions are non-negative, and their important property is that they constitute a partition of unity, $\sum_{i=1}^{n}R_{i,p}(\xi)=1$, $\forall\xi$, which makes B-spline be the basis for the approximate displacement field. The NURBS surface of order p in ξ direction and order q in η direction is defined as Eq. (25) in which $\mathbf{B}_{ij}$ and w_{ij} are the control mesh net of $n\times m$ control points, and the corresponding weights, respectively. $N_{i,p}(\xi)$ is B-spline basis function defined on the Ξ and $M_{j,q}(\eta)$ is B-spline basis function defined on the H knot vector.

$$\begin{aligned}\mathbf{S}(\xi,\eta)&=\sum_{i=1}^{n}\sum_{j=1}^{m}\frac{N_{i,p}(\xi)M_{j,q}(\eta)w_{ij}}{\sum_{i=1}^{n}\sum_{j=1}^{m}N_{i,p}(\xi)M_{j,q}(\eta)w_{ij}}\mathbf{B}_{ij}\\&=\sum_{i=1}^{n}\sum_{j=1}^{m}R_{i,j}^{p,q}(\xi,\eta)\mathbf{B}_{ij}\end{aligned} \tag{25}$$

In Eqs. (21) and (25), $R_i^p(\xi)$ and $R_{i,j}^{p,q}(\xi,\eta)$ represent the univariate and bivariate NURBS basis functions for the curve and surface, respectively. By applying the quotient rule, the first derivative of $R_{i,j}^{p,q}(\xi,\eta)$ with respect to each parametric variable (for example ξ) can be obtained as

$$\frac{\partial R_{i,j}^{p,q}(\xi,\eta)}{\partial\xi}=\frac{\frac{\partial N_{i,p}(\xi)}{\partial\xi}M_{j,q}(\eta)w_{ij}W(\xi,\eta)-\frac{\partial W(\xi,\eta)}{\partial\eta}N_{i,p}(\xi)M_{j,q}(\eta)w_{ij}}{\left(W(\xi,\eta)\right)^2} \tag{26}$$

where

$$W(\xi,\eta)=\sum_{i=1}^{n}\sum_{j=1}^{m}N_{i,p}(\xi)M_{j,q}(\eta)w_{ij} \tag{27}$$

and

$$\frac{\partial W(\xi,\eta)}{\partial\xi}=\sum_{i=1}^{n}\sum_{j=1}^{m}\frac{\partial N_{i,p}(\xi)}{\partial\xi}M_{j,q}(\eta)w_{ij} \tag{28}$$

The higher order derivatives of the NURBS functions can be derived in a similar way.

2.4 NURBS-based finite element formulation

The interpolation of dependent displacement variables in the physical space can be performed by the rational basis function of NURBS surfaces

$$u_0(x,y)=\sum_{j=1}^{nCP}u_jR_j\left(x(\xi,\eta),y(\xi,\eta)\right) \tag{29}$$

$$v_0(x,y)=\sum_{j=1}^{nCP}v_jR_j\left(x(\xi,\eta),y(\xi,\eta)\right) \tag{30}$$

$$w_0(x,y)=\sum_{j=1}^{nCP}w_jR_j\left(x(\xi,\eta),y(\xi,\eta)\right) \tag{31}$$

$$\phi_x(x,y)=\sum_{j=1}^{nCP}\phi_{xj}R_j\left(x(\xi,\eta),y(\xi,\eta)\right) \tag{32}$$

$$\phi_y(x,y)=\sum_{j=1}^{nCP}\phi_{yj}R_j\left(x(\xi,\eta),y(\xi,\eta)\right) \tag{33}$$

where *nCP* is the number of control points in the element, R_j is NURBS basis function, and (u_j, v_j, w_j, ϕ_{xj}, u_{yj}) are the displacements of control points in the homogenous space. The global set of discrete equations for this nonlinear problem can be derived in matrix form by substitution of the interpolating Eqs. (29)-(33) into the weak form of Eqs. (A1)-(A5) obtained for postbuckling analysis of graphene sheet

$$\left[\mathbf{K}\left(\mathbf{q}+w^*\right)\right]\mathbf{q}=F \tag{34}$$

The following nonlinear equation can be formed for finding the solution

$$\left[\mathbf{K}_T\left(\mathbf{q}+w^*\right)\right]\delta\mathbf{q}=-\left[R\left(\mathbf{q}+w^*\right)\right] \tag{35}$$

where $\mathbf{K}_T$, R and $\delta\mathbf{q}$ are tangent stiffness matrix, the residual load vector and the increment of the displacement, respectively. The nonlinear equations can be solved using Newton-Raphson iterative method. Although, more details of this scheme can be found in the literature (Reddy, 2014), a brief explanation is provided below. The incremental displacement vector at the *i*-th iteration is found by the following equation (Le-Manh and Lee 2014)

$$\delta\mathbf{q}^{(r)}=-\left[\mathbf{K}_T\left(w^*+\mathbf{q}^{(r-1)}\right)\right]^{-1}R\left(w^*+\mathbf{q}^{(r-1)}\right) \tag{36}$$

where R and $\mathbf{K}_T$ at the (r-1)-th iteration are obtained as follows

$$R\left(w^*+\mathbf{q}^{(r-1)}\right)=\bar{F}^{(r-1)}-\bar{F}^{(O)}-F \tag{37}$$

$$\bar{F}^{(r-1)}=\mathbf{K}\left(w^*+\mathbf{q}^{(r-1)}\right)\left\{w^*+\mathbf{q}^{(r-1)}\right\} \tag{38}$$

$$\mathbf{K}_T\left(w^*+\mathbf{q}^{(r-1)}\right)=\left.\frac{\partial R\left(w^*+\mathbf{q}^{(r-1)}\right)}{\partial\mathbf{q}}\right|_{\mathbf{q}^{(r-1)}} \tag{39}$$

where F and $\bar{F}$ are load vector and the equivalent load vector, respectively. The displacement and total displace-ent vector at the *r*-th iteration are obtained as

$$\mathbf{q}^{(r)}=\mathbf{q}^{(r-1)}+\delta\mathbf{q}^{(r)} \tag{40}$$

$$\bar{\mathbf{q}}^{(r)}=\mathbf{q}^{(r)}+w^* \tag{41}$$

The iterations in the calculations are continued until the convergence within the error tolerance 10^{-3} is satisfied. The error norm used for checking the convergence is given by

$$err=\sqrt{\frac{\sum_{i=1}^{N}\left|q_i^{r+1}-q_i^{r}\right|^2}{\sum_{i=1}^{N}\left|q_i^{r}\right|^2}}\langle 10^{-3} \tag{42}$$

where, N and q_i^r stand for the total degree of freedom and the *i*-th component of displacement vector $\mathbf{q}^r$, respectively.

3. Results and discussion

In this section, the postbuckling analysis of defective graphene sheet under symmetrically biaxial in-plane loading (Fig. 1) is presented in order to investigate the effect of out-of-plane defects on the postbuckling equilibrium paths. Here, the graphene sheet is modeled as an isotropic material and the results are presented based on the following properties (Soleimani *et al*. 2016)

$$\begin{gathered}E_1=E_2=1000\ Gpa,\quad \mathrm{G}_{12}=431.03\ \mathrm{Gpa},\\ \nu_{12}=0.16,\quad \mathrm{h}=0.34\ \mathrm{nm}\end{gathered} \tag{43}$$

The shear correction factor, k_s is set to be 5/6 and the simply supported boundary conditions are considered for graphene nanoplates and are given as follow

$$\begin{aligned}\text{SSSS: } \mathrm{u}_0=w_0=\phi_x=0 &\quad \text{at y=0 and b}\\ \nu_0=w_0=\phi_y=0 &\quad \text{at x=0 and a}\end{aligned}$$

In order to investigate the postbuckling analysis of defective graphene sheet in other boundary conditions, the postbuckling behavior are studied for SCSC and CCCC boundary conditions. Here the SCSC and CCCC boundary conditions are defined as follow

$$\begin{aligned}\text{SCSC: } \mathrm{u}_0=w_0=\phi_x=\phi_y=0 &\quad \text{at y=0 and b}\\ \nu_0=w_0=\phi_y=0 &\quad \text{at x=0 and a}\\ \text{CCCC: } \mathrm{u}_0=w_0=\phi_x=\phi_y=0 &\quad \text{at y=0 and b}\\ \nu_0=w_0=\phi_x=\phi_y=0 &\quad \text{at x=0 and a}\end{aligned}$$

It should be noted that a graphene sheet with the size of 5×5 nm is considered for SSSS boundary conditions while a 10×10 nm nanoplate is chosen for SCSC and CCCC boundary conditions.

The out-of-plane defect of SLGS which is presented as an initial geometrical imperfection, $w^*(x, y)$, is defined as a three-dimensional surface. In this study, a generic model which takes the form of products of hyperbolic and trigonometric functions is applied to simulate various possible imperfection modes. The assumed general function have controllable parameters and is presented for initial imperfection as follows (Jalali *et al*. 2016, Yang *et al*. 2006)

$$\begin{aligned}w^*(x,y)=\Gamma h\,\mathrm{sech}\left[\delta\left(\frac{x}{a}-\psi_1\right)\right]\cos\left[\mu_1\pi\left(\frac{x}{a}-\psi_1\right)\right]\times\\ \mathrm{sech}\left[\delta\left(\frac{y}{b}-\psi_2\right)\right]\cos\left[\mu_2\pi\left(\frac{y}{b}-\psi_2\right)\right]\end{aligned} \tag{44}$$

where $\psi_1=\frac{x_c}{a}$, $\psi_2=\frac{y_c}{b}$, and Γ is non-dimensional maximum amplitude of the initially defected geometry or amplitude to thickness ratio. The half-wave numbers of the imperfection in the direction of x and y axes are introduced by μ_1 and μ_2, respectively. It should be noted that the trigonometric cosine functions create a transverse bulge with the dimensionless maximum amplitude Γ and the maximum location at (x_c, y_c) while the extension of bulge on the surface of SLGS would be controlled by changing δ

parameter in hyperbolic functions. As shown in Fig. 2, when $\delta = 0$, the transverse bulge is fully extended and increasing of δ localizes the bulge to the point (x_c, y_c). In order to obtain more comprehensive results, non-dimensional postbuckling load and non-dimensional lateral deflection are defined as

$$\bar{N} = N \frac{12b^2\left(1-\nu^2\right)}{\pi E_1 h^3} \tag{45}$$

$$\bar{w}_c = \frac{w_{0c}}{h} \tag{46}$$

where w_{0c} is the additional mid-plane deflection in the center of nanoplate.

In this study, two types of out-of-plane defects defined by Eq. (55) have been studied which are presented in Fig. 3.

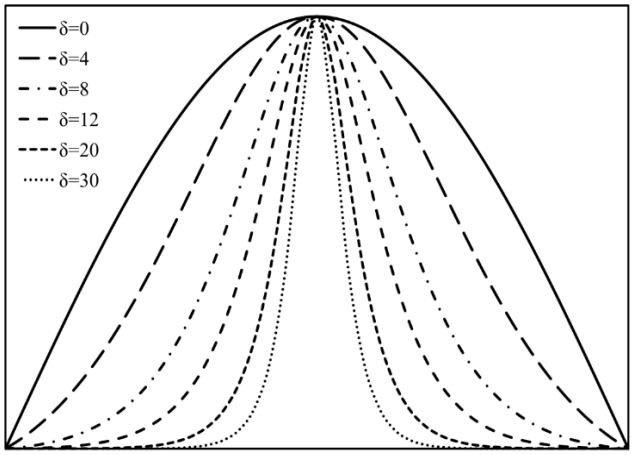

Fig. 2 Controlling of the extension of bulge on the surface of SLGS by changing δ parameter

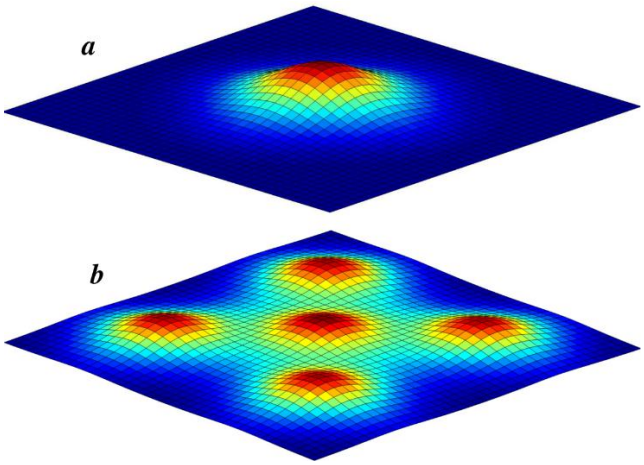

Fig. 3 Schematic diagram of two types of out-of-plane defects: (a) bulge defect with $\delta = 8$, $\mu_1 = \mu_2 = 1$, $\psi_1 = \psi_2 = 0.5$ and $\Gamma = 0.5$; (b) five bulge defects with $\delta = 10$, $\mu_1 = \mu_2 = 1$, $\Gamma = 0.5$ and $(\psi_1 = \psi_2) = (0.25, 0.25), (0.5, 0.5), (0.75, 0.75), (0.25, 0.75), (0.75, 0.25)$

Convergence test of IGA method is shown in Figs. 4 and 5 for local and nonlocal postbuckling analysis of simply supported isotropic imperfect graphene sheet under biaxial in-plane loading, respectively. For evaluating the postbuckling equilibrium paths, quadratic NURBS elements with different number of control points for each edge of graphene sheet (n) are used. The initial geometrical imperfection of graphene sheet is considered as a bulge defect with $\delta = 8$, $\psi_1 = \psi_2 = 0.5$, $\mu_1 = \mu_2 = 1$, and $\Gamma = 0.1$. It can be seen from these figures that for more number of distributed control points over each edge of the graphene nanoplate, the postbuckling paths tend to each other. As can be found, for control points of 11 on each edge, a considerable convergence can be observed for both local and nonlocal results.

In order to validate the accuracy of the proposed method, the effect of aspect ratio (b/a) on postbuckling behavior of simply supported armchair perfect graphene sheet with properties of $E_1 = 1949$ GPa, $E_2 = 1962$ GPa, $G_{12} = 846$ GPa and $\nu_{12} = 0.201$ is studied and results are given in Table 1. For the purpose of comparison, the results of Naderi and Saidi (2014) for a graphene sheet subjected to symmetrical biaxial loading are also given in Table 1. In Naderi and Saidi's work, the edge length (a), nonlocal parameter (μ) and nanoplate thickness (h) are considered to be 10, 0.04 and 0.156 nm, respectively. For each aspect

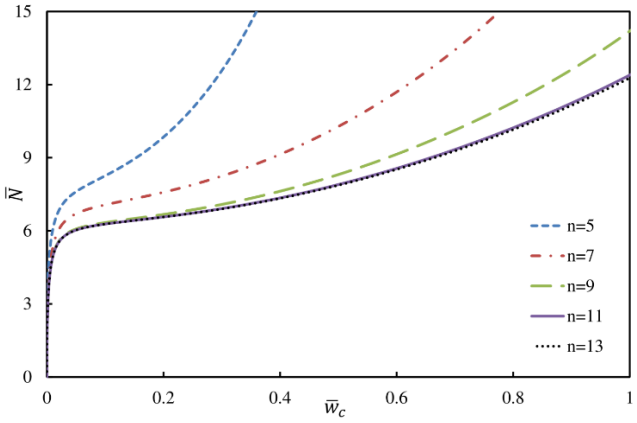

Fig. 4 Convergence test of IGA method for local analysis

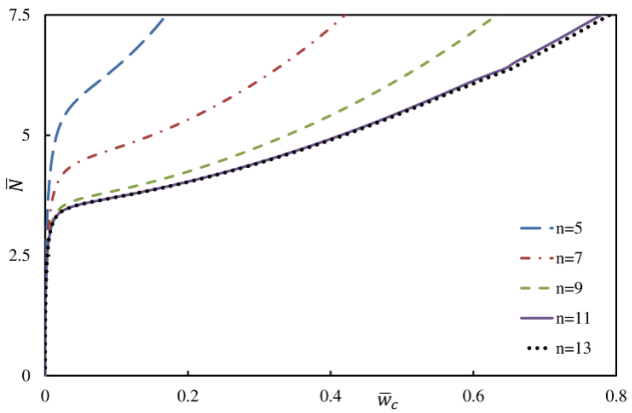

Fig. 5 Convergence test of IGA method for nonlocal analysis ($\mu = 0.2$)

Table 1 Effect of the aspect ratio on the postbuckling behavior of simply supported armchair graphene sheet

b/a	$\bar{w}_c$	(m', n')	N (nN/nm)	
			Present: IGA	Ref. (Naderi and Saidi 2014)
0.25	0	(1,1)	1.092	1.020
	0.5		1.260	1.191
	1		1.801	1.704
0.5	0	(1,1)	0.321	0.316
	0.5		0.361	0.354
	1		0.475	0.469
0.75	0	(1,1)	0.199	0.178
	0.5		0.202	0.194
	1		0.255	0.245
1	0	(1,1)	0.135	0.128
	0.5		0.149	0.140
	1		0.181	0.173

ratio, the postbuckling loads are found for three values of non-dimensional lateral deflection and first mode of buckling (m', n' are half wave numbers in the x and y directions, respectively). There is a good agreement between the results of present study and those obtained by Naderi and Saidi (2014). It is also observed that by increasing the aspect ratio of the nanoplate, the postbuckling loads decrease.

Figs. 6 and 7 show compressive postbuckling equilibrium paths of both perfect and imperfect graphene sheets based on local and nonlocal analyses, respectively for SSSS boundary conditions. In perfect case, an initial imperfection (with small amplitude) is considered to create a deviation in the plate in order to obtain postbuckling path. The smaller the deviation, the more distinct value for the critical buckling load is observed. For imperfect case, a bulge defect with $\delta = 8$, $\psi_1 = \psi_2 = 0.5$, $\mu_1 = \mu_2 = 1$ and $\Gamma = 0.25$ is considered as initial geometrical imperfection. It can be seen from these figures that initially the postbuckling curves of the imperfect nanoplate are lower than their perfect counterparts before specific $\bar{w}_c$, and then cross each other at some points, so that at large enough loads, defective graphene sheet behaves stiffer than perfect one.

The effect of nonlocal parameter on the postbuckling behavior of simply supported imperfect graphene sheet with a bulge out-of-plane defect ($\delta = 8$, $\psi_1 = \psi_2 = 0.5$, $\mu_1 = \mu_2 = 1$, $\Gamma = 0.1$) is illustrated in Fig. 8. The postbuckling equilibrium path of defective graphene sheet is initially lower for higher nonlocal parameters, and as the postbuckling load increases it becomes higher. As a result, the influence of nonlocal parameter or size effect on the postbuckling response of imperfect graphene sheet seems to be important and cannot be ignored in the analysis. It is also found from this figure that in vicinity of critical buckling load, any increase in amount of external load leads to considerable deflections which demonstrate the softening

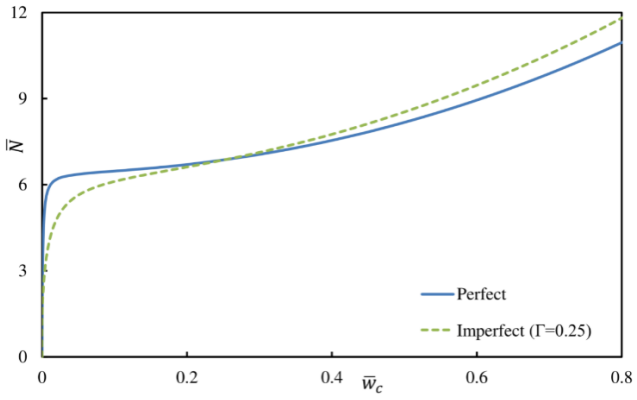

Fig. 6 Comparison of the postbuckling equilibrium paths of perfect and imperfect GSs for local analysis

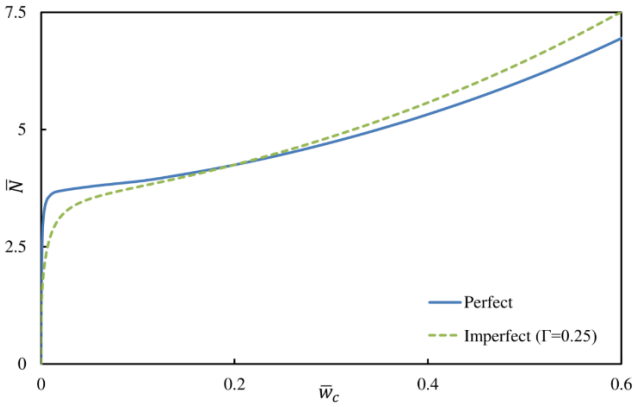

Fig. 7 Comparison of the postbuckling equilibrium paths of perfect and imperfect GSs for nonlocal analysis ($\mu = 0.2$)

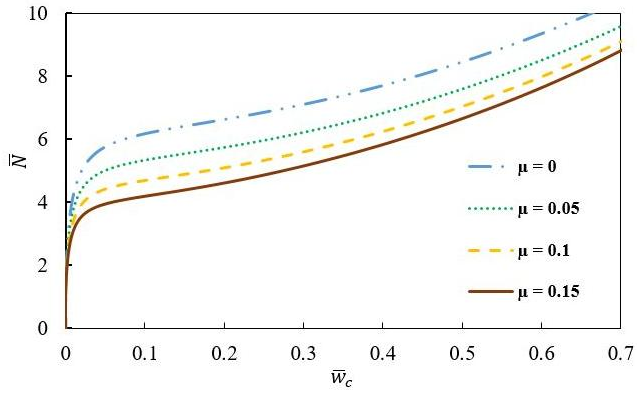

Fig. 8 Effect of nonlocal parameter on the postbuckling behavior of imperfect GS with a bulge out-of-plane defect

effect of the graphene sheet. However, far from critical buckling load, no considerable deflection is observed and the graphene sheet shows stiffer behavior. In addition, as can be seen in this figure, there is a sudden jump in nonlocal postbuckling path. This sudden change shows the stiffness behavior of the structure by increasing load and happens more suddenly by increasing nonlocal parameter

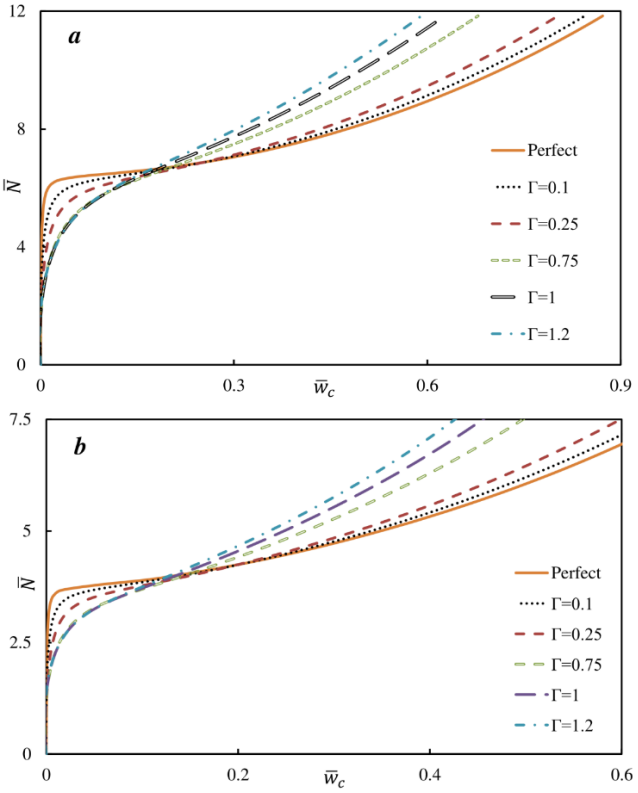

Fig. 9 Effect of imperfection amplitude on the (a) local; and (b) nonlocal (μ = 0.2) postbuckling equilibrium path of SSSS defective GS

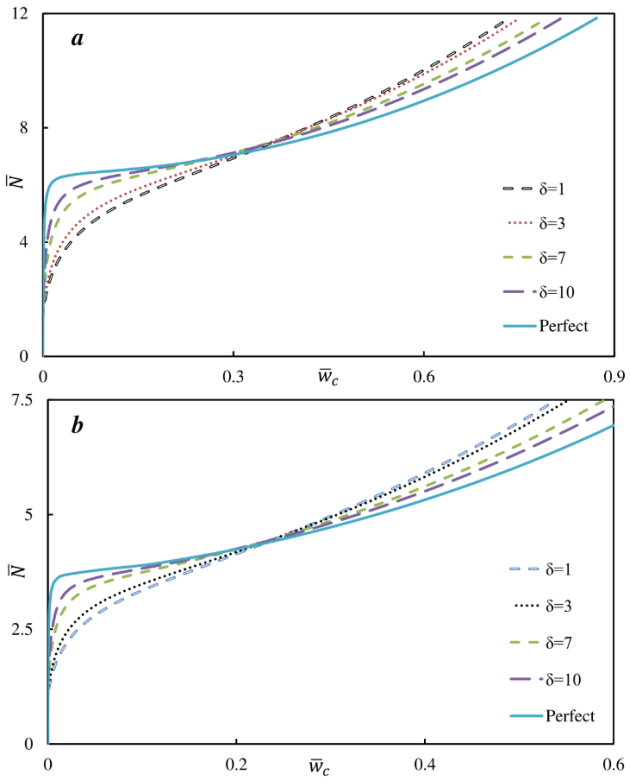

Fig. 10 Influence of imperfection extension parameter on the (a) local; and (b) nonlocal (μ = 0.2) postbuckling equilibrium path of SSSS defective GS

(μ) which reflects size effects.

Figs. 9(a) and (b) display local and nonlocal postbuckling equilibrium paths of simply supported imperfect graphene sheet with different imperfection amplitudes in order to study the effect of imperfection amplitude on the postbuckling behavior of defective graphene nanoplate with a bulge out-of-plane defect (δ = 8, ψ_1 = ψ_2 = 0.5, μ_1 = μ_2 = 1). It can be found from these figures that increasing of the imperfection amplitude initially reduces the postbuckling path of nanoplate, and as the postbuckling load increases the postbuckling curve becomes higher for nanoplate and the GS stiffness increases. Also, Figs. 9(a) and (b) illustrate that the postbuckling equilibrium path of perfect nanoplate is closer to the postbuckling curve of imperfect nanoplate for smaller imperfection amplitude.

The influence of the extension of out-of-plane defect on the postbuckling behavior of simply supported imperfect SLGSs is presented in Figs. 10(a) and (b) for local and nonlocal analyses, respectively. The postbuckling equilibrium paths of imperfect graphene nanoplate with a bulge out-of-plane defect (ψ_1 = ψ_2 = 0.5, μ_1 = μ_2 = 1, Γ = 0.25) are depicted for several values of δ parameter. It can be observed from these figures that the postbuckling load-carrying capacity is initially most weakened by decreasing of δ parameter, and as the external load increases the postbuckling load-carrying capacity increases for smaller δ parameter and the graphene sheet shows stiffer behavior.

In order to investigate the postbuckling behavior of imperfect graphene sheet with a bulge defect in different boundary conditions, postbuckling equilibrium paths in various Γ and δ for SCSC and CCCC boundary conditions are presented in Figs. 11-14. As can be seen from Figs. 11 and 12, similar to Fig. 9, the postbuckling paths of SCSC and CCCC nanoplates reduce initially by increasing of Γ, and as the postbuckling load increases the postbuckling curve becomes higher for nanoplate. Moreover, as shown in Figs. 13 and 14, the effect of δ on the postbuckling response Figs. 15 and 16, illustrate the effect of defect location on the postbuckling curves of SSSS defective graphene sheet for local and nonlocal analyses, respectively. An out-of-plane defect with δ = 8, μ_1 = μ_2 = 1, ψ_2 = 0.5 and Γ = 0.25 is assumed to move from the point ψ_1 = 0.1 to the center of plate (ψ_1 = 0.5). The postbuckling equilibrium paths are plotted for different values of defect location. As can be seen, by increasing of the ψ_1 from 0.1 to 0.3, the postbuckling curve of defective graphene sheet is slightly lower for higher ψ_1 and as expected, the central lateral deflections of nanoplate related to these defect locations are negative. Also, similar result is obtained for ψ_1 equal to 0.4 and 0.5, and the postbuckling curve of graphene sheet is slightly lower for larger ψ_1. It should be noted that in the cases of 0.4 and 0.5 the central lateral deflections of nanoplate are positive. Overall, the postbuckling strengths of defective GS with ψ_1 = 0.1 □ 0.3 are close together and similarly for ψ_1 = 0.4, 0.5. From this figure it can be concluded that the direction of central deflection of graphene sheet was changed by moving the geometric center of defect (ψ_1) from edge to center of plate.

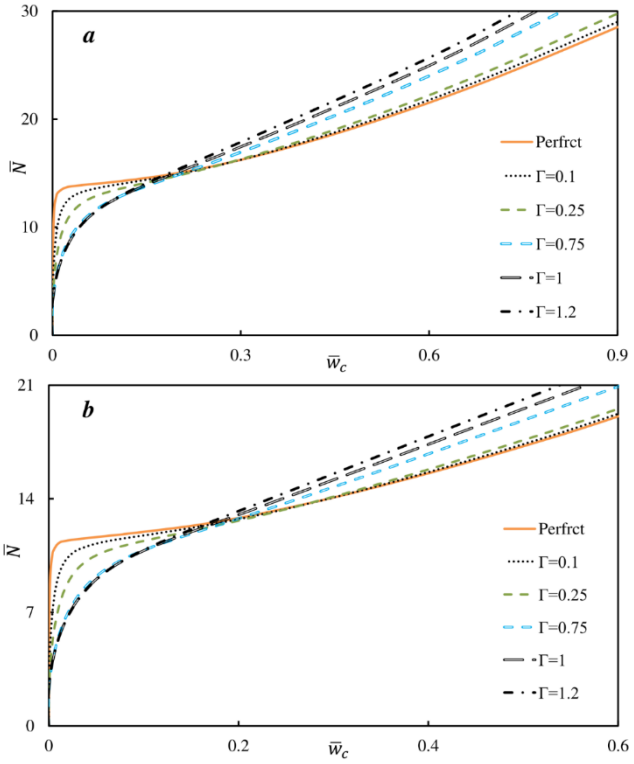

Fig. 11 Effect of imperfection amplitude on the (a) local; and (b) nonlocal (μ = 0.2) postbuckling equilibrium path of SCSC defective GS (δ = 8, $\psi_1 = \psi_2$ = 0.5, $\mu_1 = \mu_2$ = 1)

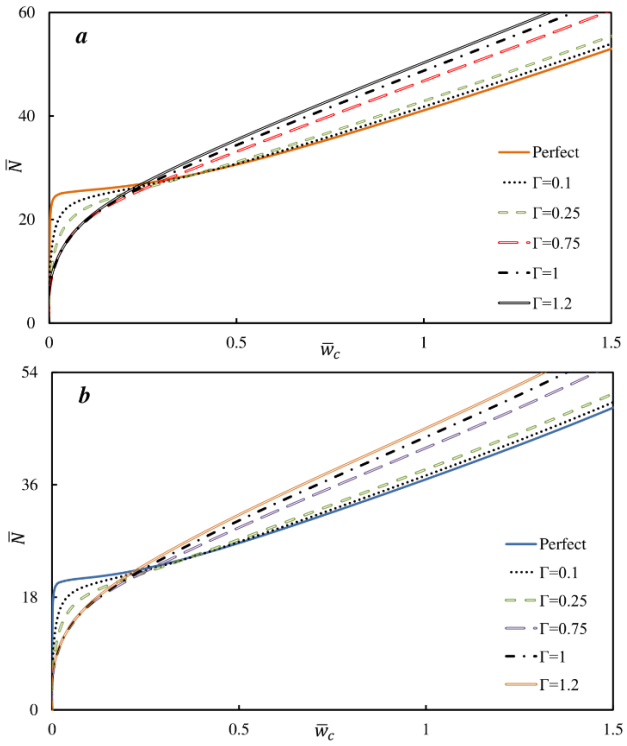

Fig. 12 Effect of imperfection amplitude on the (a) local; and (b) nonlocal (μ = 0.2) postbuckling equilibrium path of CCCC defective GS (δ = 8, $\psi_1 = \psi_2$ = 0.5, $\mu_1 = \mu_2$ = 1)

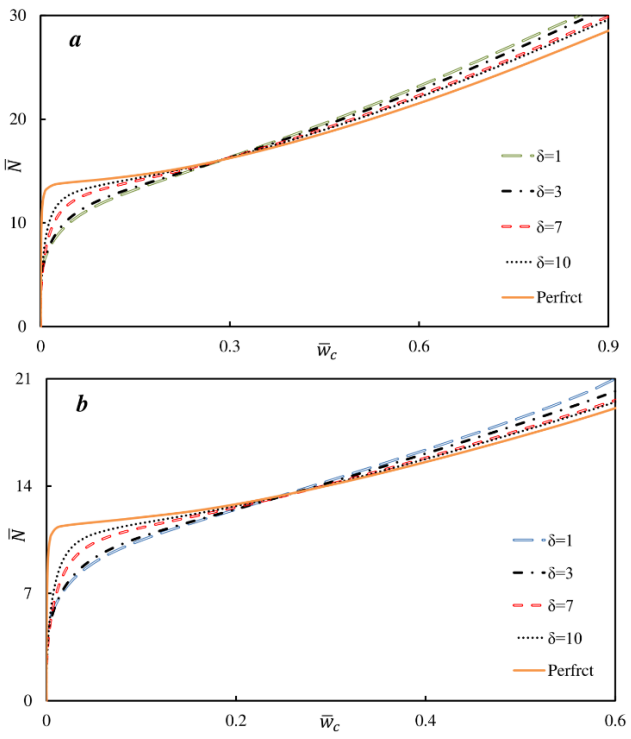

Fig. 13 Influence of imperfection extension parameter on the (a) local; and (b) nonlocal (μ = 0.2) postbuckling equilibrium path of SCSC defective GS ($\psi_1 = \psi_2$ = 0.5, $\mu_1 = \mu_2$ = 1, Γ = 0.25)

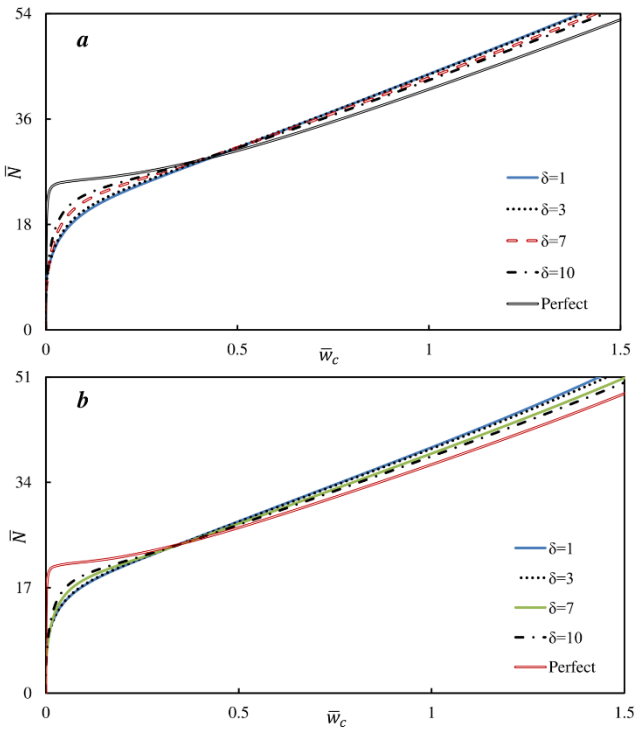

Fig. 14 Influence of imperfection extension parameter on the (a) local; and (b) nonlocal (μ = 0.2) postbuckling equilibrium path of CCCC defective GS ($\psi_1 = \psi_2$ = 0.5, $\mu_1 = \mu_2$ = 1, Γ = 0.25)

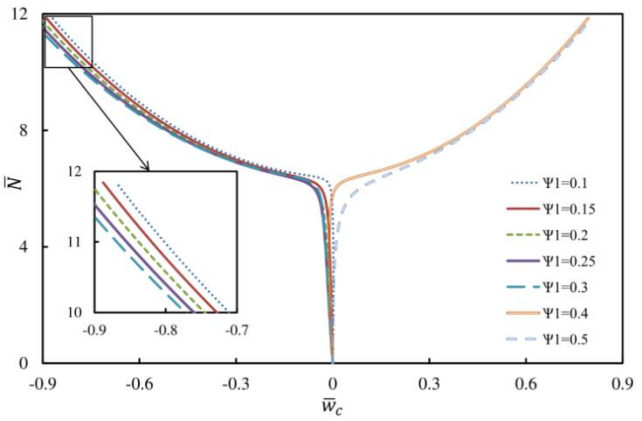

Fig. 15 Effect of imperfection location on the local postbuckling behavior of SLGS with a bulge out-of-plane defect

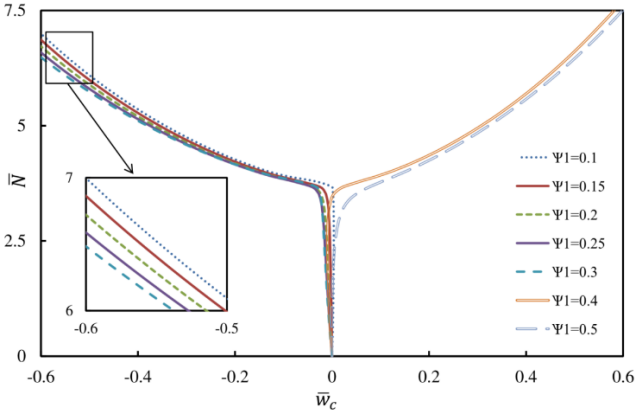

Fig. 16 Effect of imperfection location on the nonlocal postbuckling behavior of SLGS with a bulge out-of-plane defect (μ = 0.2)

In the following, the results of imperfect GS with five bulge defects with (ψ_1, ψ_2) equals to (0.25, 0.25), (0.5, 0.5), (0.75, 0.75), (0.25, 0.75), and (0.75, 0.25) (Fig. 3(b)) dispersed on the surface of graphene sheet are discussed. In these five bulge defects, $\mu_1 = \mu_2 = 1$ and $\delta = 12$. Figs. 17 and 18 demonstrate the local and nonlocal postbuckling sensitivity of SSSS GS to five bulge defects with $\Gamma = 0.6$, respectively. As expected, the postbuckling load-carrying capacity is initially lower and as the external load increases it is higher than perfect one and the graphene sheet shows stiffer behavior.

The influence of imperfection amplitude of imperfect GS with five bulge defects ($\mu_1 = \mu_2 = 1$, $\delta = 12$) on the postbuckling behavior of SSSS GS is shown in Figs. 19 and 20 for local and nonlocal analyses, respectively. As can be seen from these figures, for postbuckling curve of GS under the perfect path, the distance between perfect and imperfect curves increases for $\Gamma = 0.1$ □ 0.4, but decreases for $\Gamma > 0.4$. Also, it should be noted that as the external load increases, the perfect and imperfect paths cross each other and for postbuckling curves upper the perfect path, the distance of perfect and imperfect curves increases by increasing Γ and the postbuckling strength of SLGS will be higher.

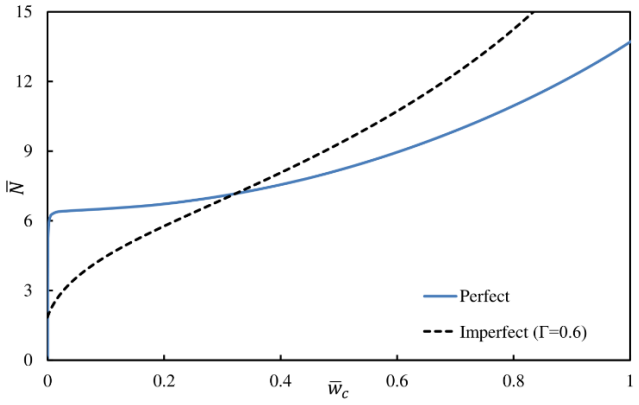

Fig. 17 Sensitivity of local postbuckling equilibrium path of SLGS to initial imperfection (five bulge defects)

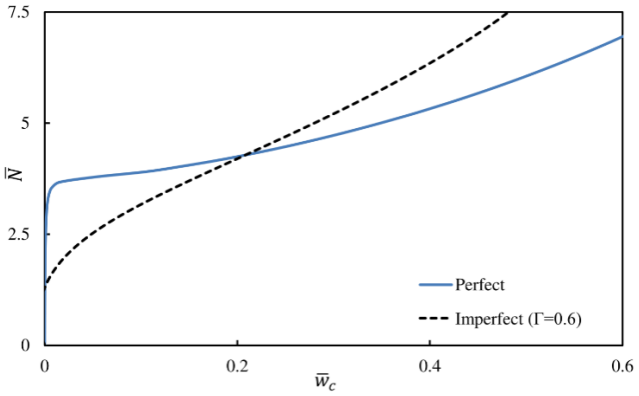

Fig. 18 Sensitivity of nonlocal postbuckling equilibrium path of SLGS to initial imperfection (μ = 0.2)

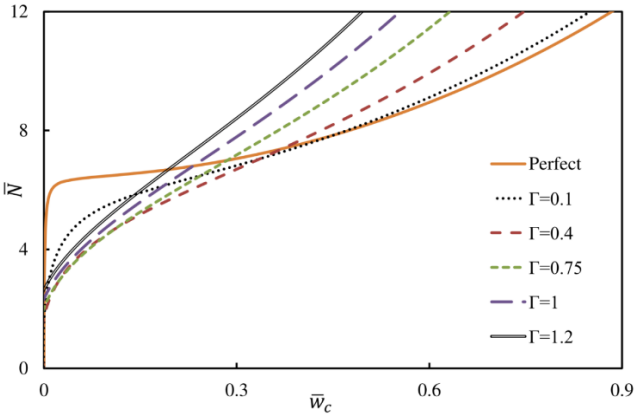

Fig. 19 Effect of imperfection amplitude on the local postbuckling behavior of SLGS with five bulge defects

In order to study the small scale effect on the postbuckling equilibrium paths of SSSS imperfect SLGS with five bulge defects ($\mu_1 = \mu_2 = 1$, $\delta = 12$, $\Gamma = 0.2$) postbuckling curves are plotted for different nonlocal parameters in Fig. 21. It can be found from this figure that the postbuckling curves of imperfect GS are initially lower for higher nonlocal parameters, and as the external load

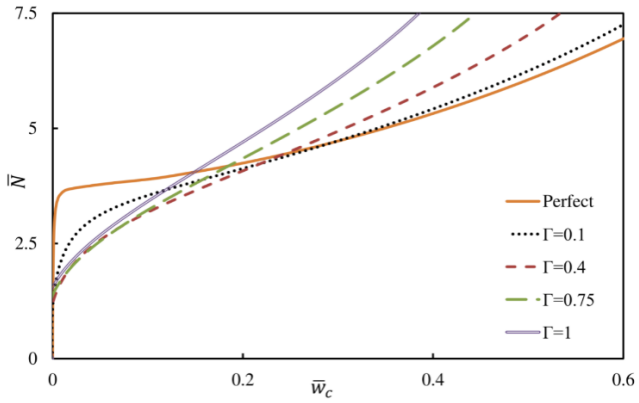

Fig. 20 Effect of imperfection amplitude on the nonlocal postbuckling behavior of SLGS with five bulge defects (μ = 0.2)

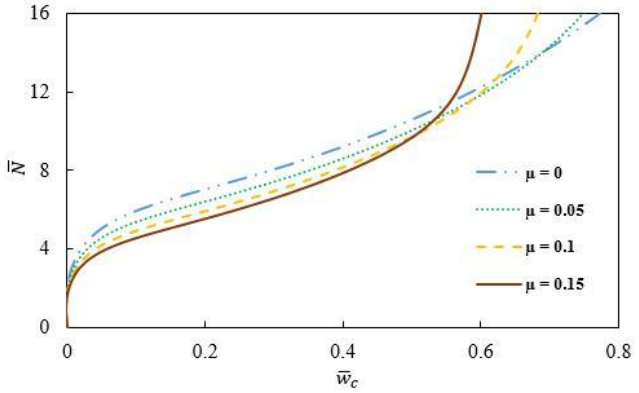

Fig. 21 Influence of nonlocal parameter on the postbuckling paths of imperfect SLGS with five bulge defects

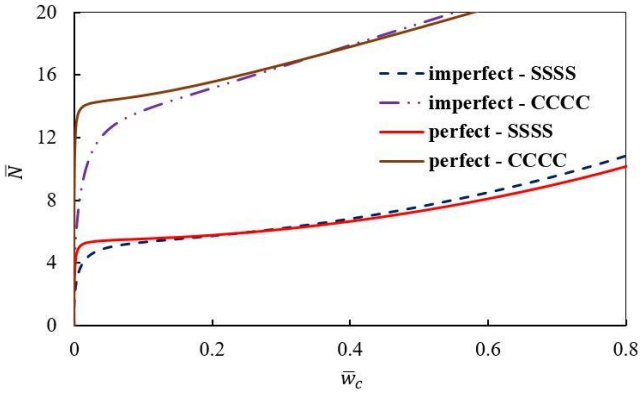

Fig. 22 Influence of imperfect SLGS with a bulge defects on the postbuckling paths with various boundary conditions

increases they become higher. It should be noted that the effect of nonlocal parameter on the postbuckling behavior of imperfect SLGS with five bulge defects is important and cannot be ignored.

Fig. 22 investigated influence of imperfect SLGS with a bulge defects on the postbuckling paths for SSSS and CCCC boundary conditions. The size of SLGS is considered 5 nm × 5 nm for both boundary conditions. This figure demonstrated SSSS is a flexible boundary condition than CCCC. Moreover, the postbuckling curve of imperfect is lower than perfect SLGS.

4. Conclusions

The sensitivity of postbuckling response of SLGS under uniform edge compression to initial imperfections (out-of-plane defects) has been investigated in this paper using nonlinear nonlocal FSDT-based isogeometric plate model. The effects of various controllable imperfection parameters such as amplitude, extension on the surface, and location of initial imperfection on the postbuckling behaviour of graphene sheet were studied and the following results are obtained:

- The postbuckling curves of the imperfect GSs are initially lower than perfect counterparts while as the external load increases, the imperfect postbuckling curves are higher.
- The imperfect postbuckling paths initially decrease by increasing of the imperfection amplitude for GS with a bulge defect, and then increase after certain points as the external load increases for both one and five bulge defects. Moreover, the postbuckling curves of perfect and imperfect graphene nanoplate with small imperfection amplitude are closer to each other.
- The postbuckling load-carrying capacity of GS is initially low for small extension parameter of imperfection and then increases by increasing of the postbuckling load.
- The postbuckling curves of perfect and imperfect GSs with high extension parameters of imperfection are closer to each other.
- The direction of central deflection of GS is changed by moving the geometric center of imperfection from edge to center of nanosheet with a bulge defect.
- The postbuckling load-carrying capacity of imperfect GS is initially lower for higher nonlocal parameters and then as the external load increases, the postbuckling strength increases. Therefore, it can be concluded that the effect of small scale is very important and cannot be ignored in the analysis.
- Finally, the postbuckling strength of defective GSs is initially lower than perfect one and as the external load increases, it is higher.

References

Adeli, M.M., Hadi, A., Hosseini, M. and Gorgani, H.H. (2017), "Torsional vibration of nano-cone based on nonlocal strain gradient elasticity theory", *Eur. Phys. J. Plus*, **132**(9), 393.

Ahouel, M., Houari, M.S.A., Bedia, E. and Tounsi, A. (2016), "Size-dependent mechanical behavior of functionally graded trigonometric shear deformable nanobeams including neutral surface position concept", *Steel Compos. Struct., Int. J.*, **20**(5),

963-981.

Ansari, R. and Norouzzadeh, A. (2016), "Nonlocal and surface effects on the buckling behavior of functionally graded nanoplates: An isogeometric analysis", *Physica E*: *Low-dimens. Syst. Nanostruct*., **84**, 84-97.

Ansari, R. and Sahmani, S. (2013), "Prediction of biaxial buckling behavior of single-layered graphene sheets based on nonlocal plate models and molecular dynamics simulations", *Appl. Math. Model*., **37**(12), 7338-7351.

Ansari, R., Sahmani, S. and Arash, B. (2010), "Nonlocal plate model for free vibrations of single-layered graphene sheets", *Phys. Lett. A*, **375**(1), 53-62.

Ansari, R., Motevalli, B., Montazeri, A. and Ajori, S. (2011), "Fracture analysis of monolayer graphene sheets with double vacancy defects via MD simulation", *Solid State Commun*., **151**(17), 1141-1146.

Ansari, R., Ajori, S. and Motevalli, B. (2012), "Mechanical properties of defective single-layered graphene sheets via molecular dynamics simulation", *Superlatt. Microstruct*., **51**(2), 274-289.

Ansari, R., Shahabodini, A. and Rouhi, H. (2013), "Prediction of the biaxial buckling and vibration behavior of graphene via a nonlocal atomistic-based plate theory", *Compos. Struct*., **95**, 88-94.

Ansari, R., Gholami, R., Sahmani, S., Norouzzadeh, A. and Bazdid-Vahdati, M. (2015), "Dynamic stability analysis of embedded multi-walled carbon nanotubes in thermal environment", *Acta Mechanica Solida Sinica*, **28**(6), 659-667.

Ansari, R., Torabi, J. and Norouzzadeh, A. (2018), "Bending analysis of embedded nanoplates based on the integral formulation of Eringen's nonlocal theory using the finite element method", *Phys. B*: *Condensed Matter*, **534**, 90-97.

Apuzzo, A., Barretta, R., Canadija, M., Feo, L., Luciano, R. and de Sciarra, F.M. (2017), "A closed-form model for torsion of nanobeams with an enhanced nonlocal formulation", *Compos. Part B*: *Eng*., **108**, 315-324.

Arda, M. and Aydogdu, M. (2018), "Longitudinal Magnetic Field Effect on Torsional Vibration of Carbon Nanotubes", *J. Computat. Appl. Mech*., **49**(2), 304-313.

Ariza, M. and Ortiz, M. (2010), "Discrete dislocations in graphene", *J. Mech. Phys. Solids*, **58**(5), 710-734.

Bağdatlı, S.M. (2015), "Non-linear vibration of nanobeams with various boundary condition based on nonlocal elasticity theory", *Compos. Part B*: *Eng*., **80**, 43-52.

Baimova, J., Bo, L., Dmitriev, S., Zhou, K. and Nazarov, A. (2013), "Effect of Stone-Thrower-Wales defect on structural stability of graphene at zero and finite temperatures", *EPL* (*Europhysics Letters*), **103**(4), 46001.

Banhart, F., Kotakoski, J. and Krasheninnikov, A.V. (2010), "Structural defects in graphene", *ACS Nano*, **5**(1), 26-41.

Belkorissat, I., Houari, M.S.A., Tounsi, A., Bedia, E. and Mahmoud, S. (2015), "On vibration properties of functionally graded nano-plate using a new nonlocal refined four variable model", *Steel Compos. Struct*., *Int. J*., **18**(4), 1063-1081.

Bodily, B. and Sun, C. (2003), "Structural and equivalent continuum properties of single-walled carbon nanotubes", *Int. J. Mater. Product Technol*., **18**(4-6), 381-397.

Bounouara, F., Benrahou, K.H., Belkorissat, I. and Tounsi, A. (2016), "A nonlocal zeroth-order shear deformation theory for free vibration of functionally graded nanoscale plates resting on elastic foundation", *Steel Compos. Struct*., *Int. J*., **20**(2), 227-249.

Brodka, A., Kołoczek, J. and Burian, A. (2007), "Application of molecular dynamics simulations for structural studies of carbon nanotubes", *J. Nanosci. Nanotechnol*., **7**(4-5), 1505-1511.

Chandra, Y., Chowdhury, R., Adhikari, S. and Scarpa, F. (2011), "Elastic instability of bilayer graphene using atomistic finite element", *Physica E*: *Low-dimens. Syst. Nanostruct*., **44**(1), 12-16.

Cottrell, J.A., Hughes, T.J. and Bazilevs, Y. (2009), *Isogeometric analysis*: *toward integration of CAD and FEA*, John Wiley & Sons.

Craighead, H.G. (2000), "Nanoelectromechanical systems", *Science*, **290**(5496), 1532-1535.

Daneshmehr, A., Rajabpoor, A. and Hadi, A. (2015), "Size dependent free vibration analysis of nanoplates made of functionally graded materials based on nonlocal elasticity theory with high order theories", *Int. J. Eng. Sci*., **95**, 23-35.

Dastjerdi, S. and Jabbarzadeh, M. (2016), "Nonlinear bending analysis of bilayer orthotropic graphene sheets resting on Winkler–Pasternak elastic foundation based on non-local continuum mechanics", *Compos. Part B*: *Eng*., **87**, 161-175.

Dastjerdi, S., Lotfi, M. and Jabbarzadeh, M. (2016), "The effect of vacant defect on bending analysis of graphene sheets based on the Mindlin nonlocal elasticity theory", *Compos. Part B*: *Eng*., **98**, 78-87.

Ebrahimi, S. (2015), "Influence of Stone–Wales defects orientations on stability of graphene nanoribbons under a uniaxial compression strain", *Solid State Commun*., **220**, 17-20.

Eringen, A.C. (1983), "On differential equations of nonlocal elasticity and solutions of screw dislocation and surface waves", *J. Appl. Phys*., **54**(9), 4703-4710.

Eringen, A.C. (2002), *Nonlocal continuum field theories*, Springer Science & Business Media.

Fan, B., Yang, X. and Zhang, R. (2010), "Anisotropic mechanical properties and Stone–Wales defects in graphene monolayer: A theoretical study", *Phys. Lett. A*, **374**(27), 2781-2784.

Fantuzzi, N. and Tornabene, F. (2016), "Strong Formulation Isogeometric Analysis (SFIGA) for laminated composite arbitrarily shaped plates", *Compos. Part B*: *Eng*., **96**, 173-203.

Farajpour, A., Shahidi, A., Mohammadi, M. and Mahzoon, M. (2012), "Buckling of orthotropic micro/nanoscale plates under linearly varying in-plane load via nonlocal continuum mechanics", *Compos. Struct*., **94**(5), 1605-1615.

Farajpour, A., Dehghany, M. and Shahidi, A. (2013a), "Surface and nonlocal effects on the axisymmetric buckling of circular graphene sheets in thermal environment", *Compos. Part B*: *Eng*., **50**, 333-343.

Farajpour, A., Solghar, A.A. and Shahidi, A. (2013b), "Postbuckling analysis of multi-layered graphene sheets under non-uniform biaxial compression", *Physica E*: *Low-dimens. Syst. Nanostruct*., **47**, 197-206.

Farajpour, M., Shahidi, A., Hadi, A. and Farajpour, A. (2018), "Influence of initial edge displacement on the nonlinear vibration, electrical and magnetic instabilities of magneto-electro-elastic nanofilms", *Mech. Adv. Mater. Struct*., 1-13.

Farzam-Rad, S.A., Hassani, B. and Karamodin, A. (2017), "Isogeometric analysis of functionally graded plates using a new quasi-3D shear deformation theory based on physical neutral surface", *Compos. Part B*: *Eng*., **108**, 174-189.

Fleck, N. and Hutchinson, J. (1997), "Strain gradient plasticity", *Adv. Appl. Mech*., **33**, 296-361.

Hadi, A., Nejad, M.Z. and Hosseini, M. (2018a), "Vibrations of three-dimensionally graded nanobeams", *Int. J. Eng. Sci*., **128**, 12-23.

Hadi, A., Nejad, M.Z., Rastgoo, A. and Hosseini, M. (2018b), "Buckling analysis of FGM Euler-Bernoulli nano-beams with 3D-varying properties based on consistent couple-stress theory", *Steel Compos. Struct*., *Int. J*., **26**(6), 663-672.

Hadi, A., Rastgoo, A., Haghighipour, N. and Bolhassani, A. (2018c), "Numerical modelling of a spheroid living cell membrane under hydrostatic pressure", *J. Statist. Mech*.: *Theory Experim*., **2018**(8), 083501.

Hao, X., Qiang, H. and Xiaohu, Y. (2008), "Buckling of defective

single-walled and double-walled carbon nanotubes under axial compression by molecular dynamics simulation", *Compos. Sci. Technol*., **68**(7), 1809-1814.

Hashimoto, A., Suenaga, K., Gloter, A., Urita, K. and Iijima, S. (2004), "Direct evidence for atomic defects in graphene layers", *Nature*, **430**(7002), 870-873.

Hosseini, M., Hadi, A., Malekshahi, A. and Shishesaz, M. (2018), "A review of size-dependent elasticity for nanostructures", *J. Computat. Appl. Mech*., **49**(1), 197-211.

Hughes, T.J., Cottrell, J.A. and Bazilevs, Y. (2005), "Isogeometric analysis: CAD, finite elements, NURBS, exact geometry and mesh refinement", *Comput. Methods Appl. Mech. Eng*., **194**(39), 4135-4195.

Ito, A. and Okamoto, S. (2012), "Mechanical properties of vacancy-containing graphene and graphite using molecular dynamics simulations", *Proceedings of the International Multi Conference of Engineers and Computer Scientists*.

Jalali, S., Pugno, N. and Jomehzadeh, E. (2016), "Influence of out-of-plane defects on vibration analysis of graphene sheets: Molecular and continuum approaches", *Superlatt. Microstruct*., **91**, 331-344.

Jamalpoor, A. and Hosseini, M. (2015), "Biaxial buckling analysis of double-orthotropic microplate-systems including in-plane magnetic field based on strain gradient theory", *Compos. Part B*: *Eng*., 75, 53-64.

Jandaghian, A.A. and Rahmani, O. (2017), "Vibration analysis of FG nanobeams based on third-order shear deformation theory under various boundary conditions", *Steel Compos. Struct., Int. J*., **25**(1), 67-78.

Jing, N., Xue, Q., Ling, C., Shan, M., Zhang, T., Zhou, X. and Jiao, Z. (2012), "Effect of defects on Young's modulus of graphene sheets: A molecular dynamics simulation", *Rsc Adv*., **2**(24), 9124-9129.

Jung, W.-Y., Han, S.-C. and Park, W.-T. (2014), "A modified couple stress theory for buckling analysis of S-FGM nanoplates embedded in Pasternak elastic medium", *Compos. Part B*: *Eng*., **60**, 746-756.

Karličić, D., Adhikari, S., Murmu, T. and Cajić, M. (2014), "Exact closed-form solution for non-local vibration and biaxial buckling of bonded multi-nanoplate system", *Compos. Part B*: *Eng*., 66, 328-339.

Kotakoski, J., Eder, F.R. and Meyer, J.C. (2014), "Atomic structure and energetics of large vacancies in graphene", *Phys. Rev. B*, **89**(20), 201406.

Le-Manh, T. and Lee, J. (2014), "Postbuckling of laminated composite plates using NURBS-based isogeometric analysis", *Compos. Struct*., **109**, 286-293.

Lehmann, T., Ryndyk, D.A. and Cuniberti, G. (2013), "Combined effect of strain and defects on the conductance of graphene nanoribbons", *Phys. Rev. B*, **88**(12), 125420.

Lherbier, A., Dubois, S.M.-M., Declerck, X., Roche, S., Niquet, Y.-M. and Charlier, J.-C. (2011), "Two-dimensional graphene with structural defects: elastic mean free path, minimum conductivity, and Anderson transition", *Phys. Rev. Lett*., **106**(4), 046803.

Li, C. and Chou, T.-W. (2003a), "Single-walled carbon nanotubes as ultrahigh frequency nanomechanical resonators", *Phys. Rev. B*, **68**(7), 073405.

Li, C. and Chou, T.-W. (2003b), "A structural mechanics approach for the analysis of carbon nanotubes", *Int. J. Solids Struct*., **40**(10), 2487-2499.

Li, L. and Hu, Y. (2015), "Buckling analysis of size-dependent nonlinear beams based on a nonlocal strain gradient theory", *Int. J. Eng. Sci*., **97**, 84-94.

Li, L. and Hu, Y. (2016), "Wave propagation in fluid-conveying viscoelastic carbon nanotubes based on nonlocal strain gradient theory", *Computat. Mater. Sci*., **112**, Part A, 282-288.

Li, L., Hu, Y. and Li, X. (2016a), "Longitudinal vibration of size-dependent rods via nonlocal strain gradient theory", *Int. J. Mech. Sci*., **115**, 135-144.

Li, L., Li, X. and Hu, Y. (2016b), "Free vibration analysis of nonlocal strain gradient beams made of functionally graded material", *Int. J. Eng. Sci*., **102**, 77-92.

Lusk, M.T., Wu, D.T. and Carr, L.D. (2010), "Graphene nanoengineering and the inverse Stone-Thrower-Wales defect", *Phys. Rev. B*, **81**(15), 155444.

Ma, J., Alfe, D., Michaelides, A. and Wang, E. (2009), "Stone-Wales defects in graphene and other planar s p 2-bonded materials", *Phys. Rev. B*, **80**(3), 033407.

Mahdavi, M., Jiang, L. and Sun, X. (2012), "Nonlinear vibration and postbuckling analysis of a single layer graphene sheet embedded in a polymer matrix", *Physica E*: *Low-dimens. Syst. Nanostruct*., **44**(7), 1708-1715.

Mohammadi, M., Farajpour, A., Moradi, A. and Ghayour, M. (2014), "Shear buckling of orthotropic rectangular graphene sheet embedded in an elastic medium in thermal environment", *Compos. Part B*: *Eng*., **56**, 629-637.

Montazeri, A., Ebrahimi, S. and Rafii-Tabar, H. (2015), "A molecular dynamics investigation of buckling behaviour of hydrogenated graphene", *Molecul. Simul*., **41**(14), 1212-1218.

Naderi, A. and Saidi, A.R. (2014), "Nonlocal postbuckling analysis of graphene sheets in a nonlinear polymer medium", *Int. J. Eng. Sci*., **81**, 49-65.

Neek-Amal, M. and Peeters, F. (2010a), "Defected graphene nanoribbons under axial compression", *Appl. Phys. Lett*., **97**(15), 153118.

Neek-Amal, M. and Peeters, F. (2010b), "Linear reduction of stiffness and vibration frequencies in defected circular monolayer graphene", *Phys. Rev. B*, **81**(23), 235437.

Neek-Amal, M. and Peeters, F. (2012), "Effect of grain boundary on the buckling of graphene nanoribbons", *Appl. Phys. Lett*., **100**(10), 101905.

Nejad, M.Z. and Hadi, A. (2016a), "Eringen's non-local elasticity theory for bending analysis of bi-directional functionally graded Euler–Bernoulli nano-beams", *Int. J. Eng. Sci*., **106**, 1-9.

Nejad, M.Z. and Hadi, A. (2016b), "Non-local analysis of free vibration of bi-directional functionally graded Euler–Bernoulli nano-beams", *Int. J. Eng. Sci*., **105**, 1-11.

Nejad, M.Z., Hadi, A. and Rastgoo, A. (2016), "Buckling analysis of arbitrary two-directional functionally graded Euler–Bernoulli nano-beams based on nonlocal elasticity theory", I*nternational J. Eng. Sci*., **103**, 1-10.

Nejad, M.Z., Hadi, A. and Farajpour, A. (2017), "Consistent couple-stress theory for free vibration analysis of Euler-Bernoulli nano-beams made of arbitrary bi-directional functionally graded materials", *Struct. Eng. Mech., Int. J*., **63**(2), 161-169.

Nguyen-Xuan, H., Thai, C.H. and Nguyen-Thoi, T. (2013), "Isogeometric finite element analysis of composite sandwich plates using a higher order shear deformation theory", *Compos. Part B*: *Eng*., **55**, 558-574.

Nguyen-Xuan, H., Tran, L.V., Thai, C.H., Kulasegaram, S. and Bordas, S.P.A. (2014), "Isogeometric analysis of functionally graded plates using a refined plate theory", *Compos. Part B*: *Eng*., **64**, 222-234.

Norouzzadeh, A. and Ansari, R. (2017), "Finite element analysis of nano-scale Timoshenko beams using the integral model of nonlocal elasticity", *Physica E*: *Low-dimens. Syst. Nanostruct*., **88**, 194-200.

Norouzzadeh, A. and Ansari, R. (2018a), "Isogeometric vibration analysis of functionally graded nanoplates with the consideration of nonlocal and surface effects", *Thin-Wall. Struct*., **127**, 354-372.

Norouzzadeh, A. and Ansari, R. (2018b), "Nonlinear dynamic

behavior of small-scale shell-type structures considering surface stress effects: An isogeometric analysis", *Int. J. Non-Linear Mech.*, **101**, 174-186.

Norouzzadeh, A., Ansari, R. and Rouhi, H. (2017), "Pre-buckling responses of Timoshenko nanobeams based on the integral and differential models of nonlocal elasticity: An isogeometric approach", *Appl. Phys. A*, **123**(5), 330.

Partovi-Azar, P., Jand, S.P., Namiranian, A. and Rafii-Tabar, H. (2013), "Electronic features induced by Stone–Wales defects in zigzag and chiral carbon nanotubes", *Computat. Mater. Sci.*, **79**, 82-86.

Piegl, L. and Tiller, W. (2012), *The NURBS book*, Springer Science & Business Media.

Pradhan, S. (2009), "Buckling of single layer graphene sheet based on nonlocal elasticity and higher order shear deformation theory", *Phys. Lett. A*, **373**(45), 4182-4188.

Radić, N. and Jeremić, D. (2016), "Thermal buckling of double-layered graphene sheets embedded in an elastic medium with various boundary conditions using a nonlocal new first-order shear deformation theory", *Compos. Part B: Eng.*, **97**, 201-215.

Rahmani, O., Refaeinejad, V. and Hosseini, S. (2017), "Assessment of various nonlocal higher order theories for the bending and buckling behavior of functionally graded nanobeams", *Steel Compos. Struct., Int. J.*, **23**(3), 339-350.

Reddy, J.N. (2014), *An Introduction to Nonlinear Finite Element Analysis: with applications to heat transfer, fluid mechanics, and solid mechanics*, OUP Oxford.

Rodrigues, J.N., Gonçalves, P., Rodrigues, N., Ribeiro, R., dos Santos, J.L. and Peres, N. (2011), "Zigzag graphene nanoribbon edge reconstruction with Stone-Wales defects", *Phys. Rev. B*, **84**(15), 155435.

Rouhi, S. and Ansari, R. (2012), "Atomistic finite element model for axial buckling and vibration analysis of single-layered graphene sheets", *Physica E: Low-dimens. Syst. Nanostruct.*, **44**(4), 764-772.

Soleimani, A., Naei, M.H. and Mashhadi, M.M. (2016), "Buckling analysis of graphene sheets using nonlocal isogeometric finite element method for NEMS applications", *Microsyst. Technol.*, 1-13.

Sun, Y., Ma, F., Ma, D., Xu, K. and Chu, P.K. (2012), "Stress-induced annihilation of Stone–Wales defects in graphene nanoribbons", *J. Phys. D: Appl. Phys.*, **45**(30), 305303.

Tang, C., Meng, L., Sun, L., Zhang, K. and Zhong, J. (2008), "Molecular dynamics study of ripples in graphene nanoribbons on 6H-SiC (0001): Temperature and size effects", *J. Appl. Phys.*, **104**(11), 113536.

Toupin, R.A. (1962), "Elastic materials with couple-stresses", *Arch. Rational Mech. Anal.*, **11**(1), 385-414.

Tran, L.V., Ferreira, A.J.M. and Nguyen-Xuan, H. (2013), "Isogeometric analysis of functionally graded plates using higher-order shear deformation theory", *Compos. Part B: Eng.*, **51**, 368-383.

Uzun, B., Numanoglu, H. and Civalek, O. (2018), "Free Vibration Analysis of BNNT with Different Cross-Sections via Nonlocal FEM", *J. Computat. Appl. Mech.*, **49**(2), 252-260.

Wang, S.-P., Guo, J.-G. and Zhou, L.-J. (2013), "Influence of Stone–Wales defects on elastic properties of graphene nanofilms", *Physica E: Low-dimens. Syst. Nanostruct.*, **48**, 29-35.

Whitener, K.E. and Sheehan, P.E. (2014), "Graphene synthesis", *Diamond and related materials*, **46**, 25-34.

Xiao, J., Staniszewski, J. and Gillespie, J. (2009), "Fracture and progressive failure of defective graphene sheets and carbon nanotubes", *Compos. Struct.*, **88**(4), 602-609.

Xiao, J., Staniszewski, J. and Gillespie, J. (2010), "Tensile behaviors of graphene sheets and carbon nanotubes with multiple Stone–Wales defects", *Mater. Sci. Eng.: A*, **527**(3), 715-723.

Yang, J., Liew, K. and Kitipornchai, S. (2006), "Imperfection sensitivity of the post-buckling behavior of higher-order shear deformable functionally graded plates", *Int. J. Solids Struct.*, **43**(17), 5247-5266.

Yin, S., Yu, T., Bui, T.Q., Zheng, X. and Tanaka, S. (2016), "In-plane material inhomogeneity of functionally graded plates: A higher-order shear deformation plate isogeometric analysis", *Compos. Part B: Eng.*, **106**, 273-284.

Zargaripoor, A., Bahrami, A. and Bahrami, M.N. (2018a), "Free vibration and buckling analysis of third-order shear deformation plate theory using exact wave propagation approach", *J. Computat. Appl. Mech.*, **49**(1), 102-124.

Zargaripoor, A., Daneshmehr, A., Hosseini, I.I. and Rajabpoor, A. (2018b), "Free vibration analysis of nanoplates made of functionally graded materials based on nonlocal elasticity theory using finite element method", *J. Computat. Appl. Mech.*, **49**(1), 86-101.

CC

Appendix A. Variational form of governing equations

Variational form of governing equations can be obtained as Eqs. (A1)-(A5).

$$\int_{A_e}\left\{\frac{\partial\delta u_0}{\partial x}\left[A_{11}\left(\frac{\partial u_0}{\partial x}+\frac{1}{2}(\frac{\partial w_0}{\partial x})^2+\frac{\partial w_0}{\partial x}\frac{\partial w^*}{\partial x}\right)+A_{12}\left(\frac{\partial v_0}{\partial y}+\frac{1}{2}(\frac{\partial w_0}{\partial y})^2+\frac{\partial w_0}{\partial y}\frac{\partial w^*}{\partial y}\right)\right]+\right.$$
$$\left.\frac{\partial\delta u_0}{\partial x}\left[A_{66}\left(\frac{\partial u_0}{\partial y}+\frac{\partial v_0}{\partial x}+\frac{\partial w_0}{\partial x}\frac{\partial w_0}{\partial y}+\frac{\partial w_0}{\partial x}\frac{\partial w^*}{\partial y}+\frac{\partial w^*}{\partial x}\frac{\partial w_0}{\partial y}\right)\right]\right\}dA-\oint_{\Gamma_e}N_n\delta u_0 ds=0 \tag{A1}$$

$$\int_{A_e}\left\{\frac{\partial\delta v_0}{\partial y}\left[A_{21}\left(\frac{\partial u_0}{\partial x}+\frac{1}{2}(\frac{\partial w_0}{\partial x})^2+\frac{\partial w_0}{\partial x}\frac{\partial w^*}{\partial x}\right)+A_{22}\left(\frac{\partial v_0}{\partial y}+\frac{1}{2}(\frac{\partial w_0}{\partial y})^2+\frac{\partial w_0}{\partial y}\frac{\partial w^*}{\partial y}\right)\right]+\right.$$
$$\left.\frac{\partial\delta v_0}{\partial x}\left[A_{66}\left(\frac{\partial u_0}{\partial y}+\frac{\partial v_0}{\partial x}+\frac{\partial w_0}{\partial x}\frac{\partial w_0}{\partial y}+\frac{\partial w_0}{\partial x}\frac{\partial w^*}{\partial y}+\frac{\partial w^*}{\partial x}\frac{\partial w_0}{\partial y}\right)\right]\right\}dA-\oint_{\Gamma_e}N_s\delta v_0 ds=0 \tag{A2}$$

$$\int_{A_e}\left\{\frac{\partial\delta w_0}{\partial x}k_sA_{55}\left(\frac{\partial(w_0+w^*)}{\partial x}+\phi_x\right)+\frac{\partial\delta w_0}{\partial y}k_sA_{44}\left(\frac{\partial(w_0+w^*)}{\partial y}+\phi_y\right)+\frac{\partial\delta w_0}{\partial x}\frac{\partial(w_0+w^*)}{\partial x}\right.$$
$$\left(A_{11}\left[\frac{\partial u_0}{\partial x}+\frac{1}{2}\left(\frac{\partial w_0}{\partial x}\right)^2+\frac{\partial w_0}{\partial x}\frac{\partial w^*}{\partial x}\right]+A_{12}\left[\frac{\partial v_0}{\partial y}+\frac{1}{2}\left(\frac{\partial w_0}{\partial y}\right)^2+\frac{\partial w_0}{\partial y}\frac{\partial w^*}{\partial y}\right]\right)+\frac{\partial\delta w_0}{\partial x}\frac{\partial(w_0+w^*)}{\partial y}$$
$$\left(A_{66}\left[\frac{\partial u_0}{\partial y}+\frac{\partial v_0}{\partial x}+\frac{\partial w_0}{\partial x}\frac{\partial w_0}{\partial y}+\frac{\partial w_0}{\partial x}\frac{\partial w^*}{\partial y}+\frac{\partial w^*}{\partial x}\frac{\partial w_0}{\partial y}\right]\right)+\frac{\partial\delta w_0}{\partial y}\frac{\partial(w_0+w^*)}{\partial y}$$
$$\left(A_{12}\left[\frac{\partial u_0}{\partial x}+\frac{1}{2}\left(\frac{\partial w_0}{\partial x}\right)^2+\frac{\partial w_0}{\partial x}\frac{\partial w^*}{\partial x}\right]+A_{22}\left[\frac{\partial v_0}{\partial y}+\frac{1}{2}\left(\frac{\partial w_0}{\partial y}\right)^2+\frac{\partial w_0}{\partial y}\frac{\partial w^*}{\partial y}\right]\right)+$$
$$\frac{\partial\delta w_0}{\partial y}\frac{\partial(w_0+w^*)}{\partial x}\left(A_{66}\left[\frac{\partial u_0}{\partial y}+\frac{\partial v_0}{\partial x}+\frac{\partial w_0}{\partial x}\frac{\partial w_0}{\partial y}+\frac{\partial w_0}{\partial x}\frac{\partial w^*}{\partial y}+\frac{\partial w^*}{\partial x}\frac{\partial w_0}{\partial y}\right]\right)+$$
$$\mu\left\{\frac{\partial^2\delta w_0}{\partial x^2}\left(A_{11}\left[\frac{\partial^2 u_0}{\partial x^2}+\frac{\partial w_0}{\partial x}\frac{\partial^2 w_0}{\partial x^2}+\frac{\partial^2 w_0}{\partial x^2}\frac{\partial w^*}{\partial x}+\frac{\partial w_0}{\partial x}\frac{\partial^2 w^*}{\partial x^2}\right]+A_{12}\left[\frac{\partial^2 v_0}{\partial x\,\partial y}+\frac{\partial w_0}{\partial y}\frac{\partial^2 w_0}{\partial x\,\partial y}+\right.\right.\right. \tag{A3}$$
$$\left.\left.\left.\frac{\partial^2 w_0}{\partial x\,\partial y}\frac{\partial w^*}{\partial y}+\frac{\partial w_0}{\partial y}\frac{\partial^2 w^*}{\partial x\,\partial y}\right]\right)\frac{\partial(w_0+w^*)}{\partial x}+\frac{\partial^2\delta w_0}{\partial x^2}\left(A_{11}\left[\frac{\partial u_0}{\partial x}+\frac{1}{2}\left(\frac{\partial w_0}{\partial x}\right)^2+\frac{\partial w_0}{\partial x}\frac{\partial w^*}{\partial x}\right]+\right.$$
$$\left.A_{12}\left[\frac{\partial v_0}{\partial y}+\frac{1}{2}\left(\frac{\partial w_0}{\partial y}\right)^2+\frac{\partial w_0}{\partial y}\frac{\partial w^*}{\partial y}\right]\right)\frac{\partial^2(w_0+w^*)}{\partial x^2}+\frac{\partial^2\delta w_0}{\partial x^2}\left(A_{66}\left[\frac{\partial^2 u_0}{\partial x\,\partial y}+\frac{\partial^2 v_0}{\partial x^2}+\right.\right.$$
$$\left.\left.\frac{\partial^2 w_0}{\partial x^2}\frac{\partial w_0}{\partial y}+\frac{\partial w_0}{\partial x}\frac{\partial^2 w_0}{\partial x\,\partial y}+\frac{\partial^2 w_0}{\partial^2 x}\frac{\partial w^*}{\partial y}+\frac{\partial w_0}{\partial x}\frac{\partial^2 w^*}{\partial x\,\partial y}+\frac{\partial^2 w^*}{\partial x^2}\frac{\partial w_0}{\partial y}+\frac{\partial w^*}{\partial x}\frac{\partial^2 w_0}{\partial x\,\partial y}\right]\right)$$
$$\frac{\partial(w_0+w^*)}{\partial y}+\frac{\partial^2\delta w_0}{\partial x^2}\left(A_{66}\left[\frac{\partial u_0}{\partial y}+\frac{\partial v_0}{\partial x}+\frac{\partial w_0}{\partial x}\frac{\partial w_0}{\partial y}+\frac{\partial w_0}{\partial x}\frac{\partial w^*}{\partial y}+\frac{\partial w^*}{\partial x}\frac{\partial w_0}{\partial y}\right]\right)\frac{\partial^2(w_0+w^*)}{\partial x\,\partial y}$$
$$+\frac{\partial^2\delta w_0}{\partial x^2}\left(A_{12}\left[\frac{\partial^2 u_0}{\partial x\,\partial y}+\frac{\partial w_0}{\partial x}\frac{\partial^2 w_0}{\partial x\,\partial y}+\frac{\partial^2 w_0}{\partial x\,\partial y}\frac{\partial w^*}{\partial x}+\frac{\partial w_0}{\partial x}\frac{\partial^2 w^*}{\partial x\,\partial y}\right]\right)$$
$$+A_{22}\left[\frac{\partial^2 v_0}{\partial y^2}+\frac{\partial w_0}{\partial y}\frac{\partial^2 w_0}{\partial y^2}+\frac{\partial^2 w_0}{\partial y^2}\frac{\partial w^*}{\partial y}+\frac{\partial w_0}{\partial y}\frac{\partial^2 w^*}{\partial y^2}\right]\Bigg)\frac{\partial(w_0+w^*)}{\partial y}+\frac{\partial^2\delta w_0}{\partial x^2}\left(A_{12}\left[\frac{\partial u_0}{\partial x}+\right.\right.$$

$$\frac{1}{2}\left(\frac{\partial w_0}{\partial x}\right)^2+\frac{\partial w_0}{\partial x}\frac{\partial w^*}{\partial x}\Bigg]+A_{22}\left[\frac{\partial v_0}{\partial y}+\frac{1}{2}\left(\frac{\partial w_0}{\partial y}\right)^2+\frac{\partial w_0}{\partial y}\frac{\partial w^*}{\partial y}\right]\Bigg)\frac{\partial^2(w_0+w^*)}{\partial y^2}$$
$$+\frac{\partial^2\delta w_0}{\partial x^2}\Bigg(A_{66}\left[\frac{\partial^2 u_0}{\partial y^2}+\frac{\partial^2 v_0}{\partial x\,\partial y}+\frac{\partial^2 w_0}{\partial x\,\partial y}\frac{\partial w_0}{\partial y}+\frac{\partial w_0}{\partial x}\frac{\partial^2 w_0}{\partial y^2}+\frac{\partial^2 w_0}{\partial x\,\partial y}\frac{\partial w^*}{\partial y}+$$
$$\frac{\partial w_0}{\partial x}\frac{\partial^2 w^*}{\partial y^2}+\frac{\partial^2 w^*}{\partial x\,\partial y}\frac{\partial w_0}{\partial y}+\frac{\partial w^*}{\partial x}\frac{\partial^2 w_0}{\partial y^2}\Bigg]\Bigg)\frac{\partial(w_0+w^*)}{\partial x}+$$
$$\frac{\partial^2\delta w_0}{\partial x^2}\Bigg(A_{66}\left[\frac{\partial u_0}{\partial y}+\frac{\partial v_0}{\partial x}+\frac{\partial w_0}{\partial x}\frac{\partial w_0}{\partial y}+\frac{\partial w_0}{\partial x}\frac{\partial w^*}{\partial y}+\frac{\partial w^*}{\partial x}\frac{\partial w_0}{\partial y}\right]\Bigg)\frac{\partial^2(w_0+w^*)}{\partial x\,\partial y}$$
$$+\frac{\partial^2\delta w_0}{\partial y^2}\Bigg(A_{11}\left[\frac{\partial^2 u_0}{\partial x^2}+\frac{\partial w_0}{\partial x}\frac{\partial^2 w_0}{\partial x^2}+\frac{\partial^2 w_0}{\partial x^2}\frac{\partial w^*}{\partial x}+\frac{\partial w_0}{\partial x}\frac{\partial^2 w^*}{\partial x^2}\right]+$$
$$A_{12}\left[\frac{\partial^2 v_0}{\partial x\,\partial y}+\frac{\partial w_0}{\partial y}\frac{\partial^2 w_0}{\partial x\,\partial y}+\frac{\partial^2 w_0}{\partial x\,\partial y}\frac{\partial w^*}{\partial y}+\frac{\partial w_0}{\partial y}\frac{\partial^2 w^*}{\partial x\,\partial y}\right]\Bigg)\frac{\partial(w_0+w^*)}{\partial x}+$$
$$\frac{\partial^2\delta w_0}{\partial y^2}\Bigg(A_{11}\left[\frac{\partial u_0}{\partial x}+\frac{1}{2}\left(\frac{\partial w_0}{\partial x}\right)^2+\frac{\partial w_0}{\partial x}\frac{\partial w^*}{\partial x}\right]+A_{12}\left[\frac{\partial v_0}{\partial y}+\frac{1}{2}\left(\frac{\partial w_0}{\partial y}\right)^2+\frac{\partial w_0}{\partial y}\frac{\partial w^*}{\partial y}\right]\Bigg)\frac{\partial^2(w_0+w^*)}{\partial x^2}+$$
$$\frac{\partial^2\delta w_0}{\partial y^2}\Bigg(A_{66}\left[\frac{\partial^2 u_0}{\partial x\,\partial y}+\frac{\partial^2 v_0}{\partial x^2}+\frac{\partial^2 w_0}{\partial x^2}\frac{\partial w_0}{\partial y}+\frac{\partial w_0}{\partial x}\frac{\partial^2 w_0}{\partial x\,\partial y}+\frac{\partial^2 w_0}{\partial^2 x}\frac{\partial w^*}{\partial y}+\frac{\partial w_0}{\partial x}\frac{\partial^2 w^*}{\partial x\,\partial y}+\frac{\partial^2 w^*}{\partial x^2}\frac{\partial w_0}{\partial y}+$$
$$\frac{\partial w^*}{\partial x}\frac{\partial^2 w_0}{\partial x\,\partial y}\Bigg]\Bigg)\frac{\partial(w_0+w^*)}{\partial y}+\frac{\partial^2\delta w_0}{\partial y^2}\Bigg(A_{66}\left[\frac{\partial u_0}{\partial y}+\frac{\partial v_0}{\partial x}+\frac{\partial w_0}{\partial x}\frac{\partial w_0}{\partial y}+\frac{\partial w_0}{\partial x}\frac{\partial w^*}{\partial y}+\frac{\partial w^*}{\partial x}\frac{\partial w_0}{\partial y}\right]\Bigg)$$
$$\frac{\partial^2(w_0+w^*)}{\partial x\,\partial y}+\frac{\partial^2\delta w_0}{\partial y^2}\Bigg(A_{12}\left[\frac{\partial^2 u_0}{\partial x\,\partial y}+\frac{\partial w_0}{\partial x}\frac{\partial^2 w_0}{\partial x\,\partial y}+\frac{\partial^2 w_0}{\partial x\,\partial y}\frac{\partial w^*}{\partial x}+\frac{\partial w_0}{\partial x}\frac{\partial^2 w^*}{\partial x\,\partial y}\right]$$
$$+A_{22}\left[\frac{\partial^2 v_0}{\partial y^2}+\frac{\partial w_0}{\partial y}\frac{\partial^2 w_0}{\partial y^2}+\frac{\partial^2 w_0}{\partial y^2}\frac{\partial w^*}{\partial y}+\frac{\partial w_0}{\partial y}\frac{\partial^2 w^*}{\partial y^2}\right]\Bigg)\frac{\partial(w_0+w^*)}{\partial y}$$
$$+\frac{\partial^2\delta w_0}{\partial y^2}\Bigg(A_{12}\left[\frac{\partial u_0}{\partial x}+\frac{1}{2}\left(\frac{\partial w_0}{\partial x}\right)^2+\frac{\partial w_0}{\partial x}\frac{\partial w^*}{\partial x}\right]+A_{22}\left[\frac{\partial v_0}{\partial y}+\frac{1}{2}\left(\frac{\partial w_0}{\partial y}\right)^2+\frac{\partial w_0}{\partial y}\frac{\partial w^*}{\partial y}\right]\Bigg)$$
$$\frac{\partial^2(w_0+w^*)}{\partial y^2}+\frac{\partial^2\delta w_0}{\partial y^2}\Bigg(A_{66}\left[\frac{\partial^2 u_0}{\partial y^2}+\frac{\partial^2 v_0}{\partial x\,\partial y}+\frac{\partial^2 w_0}{\partial x\,\partial y}\frac{\partial w_0}{\partial y}+\frac{\partial w_0}{\partial x}\frac{\partial^2 w_0}{\partial y^2}+\frac{\partial^2 w_0}{\partial x\,\partial y}\frac{\partial w^*}{\partial y}+\frac{\partial w_0}{\partial x}\frac{\partial^2 w^*}{\partial y^2}$$
$$+\frac{\partial^2 w^*}{\partial x\,\partial y}\frac{\partial w_0}{\partial y}+\frac{\partial w^*}{\partial x}\frac{\partial^2 w_0}{\partial y^2}\Bigg]\Bigg)\frac{\partial(w_0+w^*)}{\partial x}+$$
$$\frac{\partial^2\delta w_0}{\partial y^2}\Bigg(A_{66}\left[\frac{\partial u_0}{\partial y}+\frac{\partial v_0}{\partial x}+\frac{\partial w_0}{\partial x}\frac{\partial w_0}{\partial y}+\frac{\partial w_0}{\partial x}\frac{\partial w^*}{\partial y}+\frac{\partial w^*}{\partial x}\frac{\partial w_0}{\partial y}\right]\Bigg)\frac{\partial^2(w_0+w^*)}{\partial x\,\partial y}\Bigg\}\Bigg\}dA+$$
$$\oint_{\Gamma_e}\Bigg\{\delta w_0\Bigg[N\left(\frac{\partial(w_0+w^*)}{\partial x}n_x-\mu\left(\frac{\partial^3(w_0+w^*)}{\partial x^3}n_x+\frac{\partial^3 w_0}{\partial y\,\partial x^2}n_y\right)\right)+\lambda N\left(\frac{\partial(w_0+w^*)}{\partial y}n_y-$$
$$\mu\left(\frac{\partial^3(w_0+w^*)}{\partial y^3}n_y+\frac{\partial^3(w_0+w^*)}{\partial x\,\partial y^2}n_y\right)\right)-\left(Q_x n_x+Q_y n_y\right)\Bigg]+\Bigg[\frac{\partial\delta w_0}{\partial x}\Bigg(\mu N\left(\frac{\partial^2(w_0+w^*)}{\partial x^2}+$$
$$\lambda\frac{\partial^2(w_0+w^*)}{\partial y^2}\right)n_x\Bigg)+\frac{\partial\delta w_0}{\partial y}\left(\mu N\left(\frac{\partial^2(w_0+w^*)}{\partial x^2}+\lambda\frac{\partial^2 w_0}{\partial y^2}\right)n_y\right)\Bigg]\Bigg\}ds=0 \tag{A3}$$

$$\int_{A_e}\left\{\frac{\partial\delta\phi_x}{\partial x}\left[D_{11}\frac{\partial\phi_x}{\partial x}+D_{12}\frac{\partial\phi_y}{\partial y}\right]+\frac{\partial\delta\phi_x}{\partial y}\left[D_{66}\left(\frac{\partial\phi_x}{\partial y}+\frac{\partial\phi_y}{\partial x}\right)\right]+\delta\phi_x\left[k_sA_{55}\left(\frac{\partial(w_0+w^*)}{\partial x}+\phi_x\right)\right]\right\}dA - \oint_{\Gamma_e}M_n\delta\phi_n ds=0 \tag{A4}$$

$$\int_{A_e}\left\{\frac{\partial\delta\phi_y}{\partial x}\left[D_{66}\left(\frac{\partial\phi_x}{\partial y}+\frac{\partial\phi_y}{\partial x}\right)\right]+\frac{\partial\delta\phi_y}{\partial y}\left[D_{21}\frac{\partial\phi_x}{\partial x}+D_{22}\frac{\partial\phi_y}{\partial y}\right]+\delta\phi_y\left[k_sA_{44}\left(\frac{\partial(w_0+w^*)}{\partial y}+\phi_y\right)\right]\right\}dA - \oint_{\Gamma_e}M_n\delta\phi_n ds=0 \tag{A5}$$

In Eqs. (A1)-(A5)

$$N_n=N_{xx}n_x+N_{xy}n_y \tag{A6}$$

$$N_s=N_{xy}n_x+N_{yy}n_y \tag{A7}$$

$$M_n=M_{xx}n_x+M_{xy}n_y \tag{A8}$$

$$M_s=M_{xy}n_x+M_{yy}n_y \tag{A9}$$

$$N_{yy}=\lambda N_{xx}=-\lambda N,\quad N_{xy}=0 \tag{A10}$$